

ON THE NATURE OF THE HEAT SOURCE FOR DAMPED Ly α SYSTEMS

ARTHUR M. WOLFE¹ & J. CHRISTOPHER HOWK¹

DEPARTMENT OF PHYSICS AND CENTER FOR ASTROPHYSICS AND SPACE SCIENCES;
UNIVERSITY OF CALIFORNIA, SAN DIEGO;
C-0424; LA JOLLA, CA 92093
awolfe@ucsd.edu, howk@ucsd.edu

ERIC GAWISER
DEPARTMENT OF ASTRONOMY;
YALE UNIVERSITY
P.O. Box 208101
NEW HAVEN, CT 06520-8101
egawiser@astro.yale.edu

JASON X. PROCHASKA¹
UCO-LICK OBSERVATORY;
UNIVERSITY OF CALIFORNIA, SANTA CRUZ
SANTA CRUZ, CA; 95464
xavier@ucolick.org

AND
SEBASTIÁN LOPEZ
UNIVERSIDAD DE CHILE;
DEPARTAMENTO DE ASTRONOMIA
CASILLA 36-D, LAS CONDES,
SANTIAGO, CHILE
slopez@das.uchile.cl

Accepted for Publication by the Astrophysical Journal July 14, 2004

ABSTRACT

We investigate the heat source of the neutral gas comprising damped Ly α systems. Unlike the Ly α forest, where the extragalactic background radiation field ionizes and heats the gas, we find that grain photoelectric heating by the FUV background is not sufficient to balance the C II 158 μm cooling rate inferred from damped Ly α systems. In these systems, a local energy source is required. We show that in the case of the $z=1.919$ damped Ly α system toward Q2206–19, the local source is FUV emission from the associated galaxy found by Møller et al. (2002): the mean intensity inferred from photometry is in good agreement with the intensity J_{ν}^{stars} required to explain the cooling rate. The FUV mean intensity predicted for a cold neutral medium (CNM) model, $J_{\nu}^{\text{stars}} = (1.7_{-1.0}^{+2.7}) \times 10^{-18} \text{ ergs cm}^{-2} \text{ s}^{-1} \text{ Hz}^{-1} \text{ sr}^{-1}$ (95% c.l.), is the largest expected from our C II* study of 45 damped Ly α systems. This may explain why this is the only confirmed damped Ly α system yet detected in emission at $z > 1.9$. We argue that in most damped Ly α systems with detected C II* absorption, J_{ν}^{stars} is between 10^{-19} and $10^{-18} \text{ ergs cm}^{-2} \text{ s}^{-1} \text{ Hz}^{-1} \text{ sr}^{-1}$ and heats the gas which is a CNM. By contrast, in most damped Ly α systems with upper limits on C II* absorption the gas is a warm neutral medium (WNM). Surprisingly, the upper limits are compatible with the same range of J_{ν}^{stars} values suggesting the majority of damped Ly α systems are heated by radiation fields generated by a limited range of star formation rates per unit H I area, between 10^{-3} and $10^{-2} \text{ M}_{\odot} \text{ yr}^{-1} \text{ kpc}^{-2}$. We also show that C II* absorption is unlikely to arise in gas that is ionized.

Subject headings: cosmology—galaxies: evolution—galaxies: quasars—absorption lines

1. INTRODUCTION

External background radiation is the widely accepted heat source for the Ly α forest. Defined to have H I column densities $N(\text{H I}) < 10^{17} \text{ cm}^{-2}$ the Ly α forest clouds are optically thin at the Lyman limit. As a result, ionizing background radiation, i.e., radiation with photon energies $h\nu > h\nu_H = 13.6 \text{ eV}$, penetrates the interior of the clouds, ionizing them such that the neutral gas fraction $n(\text{H}^0)/n < 10^{-5}$, and heats them to temperatures in excess of 10000 K (Rauch 1998). Indeed, several authors have constructed scenarios within the context of CDM cos-

mogonies in which most of the baryons in the universe at $z \sim 3$ reside in the Ly α forest and are photoionized by background radiation (e.g., Miralda-Escudé et al. 1996; Machacek et al. 2000).

Calculations by Haardt & Madau (1996; 2003) show that radiation emitted from the integrated population of QSOs and galaxies results in a mean background intensity $J_{\nu_H} \sim 10^{-21} \text{ ergs cm}^{-2} \text{ s}^{-1} \text{ Hz}^{-1} \text{ sr}^{-1}$ at $z \sim 3$. Independent tests, such as the decrease with redshift of the number of absorbers per unit redshift in the vicinity of the QSO, i.e., “the proximity effect”, indicate similar values for J_{ν_H} (e.g., Scott et al. 2002). Ionizing background radiation has also been invoked to explain the ionization structure of metals in the Ly α forest, and in higher column-density QSO absorption systems selected for C IV $\lambda\lambda$ 1548, 1551

¹Visiting Astronomer, W.M. Keck Telescope. The Keck Observatory is a joint facility of the University of California and the California Institute of Technology.

absorption (e.g. Mo & Miralda-Escudé 1995), Lyman limit absorption (Prochaska 1999), and Mg II $\lambda\lambda$ 2796, 2803 absorption (e.g. Churchill, Vogt, & Charlton 2003). The predicted temperatures in these absorbers are also about 10000 K and the neutral gas fraction, $n(\text{H}^0)/n \ll 1$.

In this paper we consider the nature of the heat source for another class of QSO absorption systems, the damped Ly α systems (see Storrie-Lombardi & Wolfe 2000). While the damped Ly α systems are subject to the same external radiation fields as the other absorbers, they differ in one important respect: the gas is neutral (e.g. Vladilo et al. 2001; Prochaska et al. 2002). Defined to have H I column densities $N(\text{H I}) \geq 2 \times 10^{20} \text{ cm}^{-2}$, damped Ly α systems have Lyman-limit optical depths, $\tau_{\nu_H} \geq 1000$. As a result, the same photons that ionize and heat the Ly α forest do not penetrate the interior of the damped Ly α systems. Rather, these gas layers are penetrated only by background radiation with photon energies $h\nu \gtrsim 400 \text{ eV}$ and $h\nu < h\nu_H$. While the low-energy FUV photons do not ionize H, they do ionize neutral species of atoms with ionization potentials less than $h\nu_H$ such as C, Fe, and Zn, and more importantly, could contribute to the heat input of damped Ly α systems through grain photoelectric heating (Bakes & Tielens 1994). Similarly, X-ray photons can also heat the gas through photoionization.

Does such background radiation dominate the heat input to the damped Ly α systems? We shall address this question empirically since cooling rates have recently been measured for a representative sample of ~ 50 damped Ly α systems (see Wolfe, Prochaska, & Gawiser 2003, hereafter referred to as WPG, for a discussion of the original sample of 33 damped Ly α systems). The answer has important implications. If heating by external sources does not match the measured cooling rates, then internal sources of heating must be found. This would distinguish damped Ly α systems from all other classes of QSO absorption systems, which are plausibly heated by background radiation.

This paper is organized as follows. In § 2 we describe our technique for obtaining the thermal equilibria of damped Ly α systems heated by external background radiation. In particular we compute the thermal equilibria of neutral gas layers exposed to background radiation fields recently computed by Haardt & Madau (2003). These authors computed backgrounds originating from the integrated population of (1) QSOs alone, and (2) QSOs and galaxies. To maximize the heating rates we consider those backgrounds that include galaxies because the galaxy contribution dominates at $h\nu \leq h\nu_H$, where FUV radiation ($6 < h\nu < 13.6 \text{ eV}$) heats the gas by the grain photoelectric mechanism (WPG). This is the same process by which the neutral ISM of the Galaxy is heated (e.g. Bakes & Tielens 1994), and it is relevant here given the evidence for dust in damped Ly α systems (Pettini et al. 1994; Pei & Fall 1995; WPG). At $h\nu \gtrsim 400 \text{ eV}$, soft X-rays heat the gas by photoionizing H, He, and abundant elements. X-ray heating occurs primarily through the photoionization of H and He because of the low metallicities of damped Ly α systems. In § 3 we apply these results to test the background heating hypothesis. We compare the predicted heating rates to the 158 μm cooling rates deduced from the strength of C II* λ 1335.7 and damped Ly α absorption (see WPG). We study the multi-phase structure of the $z = 1.919$ damped

Ly α system toward Q2206–19, and then discuss results for the full sample of 45 damped Ly α systems. In § 4 we examine the nature of possible internal heat sources by focusing on the $z=1.919$ damped Ly α system toward Q2206–19. This damped Ly α system is ideal for such a study because the presence of an associated galaxy at the same redshift, which is detected via its rest-frame FUV emission (Møller et al. 2002), allows one to make an independent estimate of the FUV radiation field incident on the absorbing gas. Since Fe is believed to be depleted in this DLA, the radiation is incident on dust, and the result is grain photoelectric heating. WPG show how to deduce the local FUV radiation field from the strength of C II* absorption. In § 5 we investigate the energy input for all the damped Ly α systems in our sample, i.e., those with positive detections and those with upper limits on C II* absorption, to determine whether they are heated by background radiation alone or require internal heat sources. In § 6 we discuss the possibility that C II* absorption arises in ionized gas. Finally, concluding remarks are given in § 7.

Throughout this paper we adopt a cosmology consistent with the WMAP (Bennett et al. 2003) results, $(\Omega_m, \Omega_\Lambda, h) = (0.3, 0.7, 0.7)$.

2. THERMAL EQUILIBRIA OF BACKGROUND HEATED DAMPED Ly α SYSTEMS

Consider a slab of neutral gas exposed to an isotropic background radiation field with mean intensity J_ν . We first compute the heating rates due to soft X-rays and FUV radiation. We then calculate the thermal equilibria resulting from a balance between heating and cooling.

2.1. Heating

Wolfire et al. (1995; hereafter W95) find the primary ionization rate of atomic species i due to soft X-rays to be

$$\zeta_{XR}^i = 4\pi \int \frac{J_\nu}{h\nu} \exp[-\sigma_\nu N^a(\text{HI})] \sigma_\nu^i d\nu \text{ s}^{-1} \quad , \quad (1)$$

where σ_ν^i is the photoionization cross-section per H atom of species i and the factor $\sigma_\nu N^a(\text{H I})$ is the optical depth due to H, He, and abundant metals such as C, O, Fe, etc. in an attenuating column density $N^a(\text{H I})$. To simulate conditions in the midplane of the gas layer we let $N^a(\text{H I}) = 0.5N(\text{H I})$, where $N(\text{H I})$ is the H I column density detected along the line of sight. We compute the total ionization rate of H and He, including secondary ionizations, using the prescription of W95 including their modifications of the results of Shull & van-Steenberg (1985). The resulting heating rate is given by

$$\Gamma_{XR} = 4\pi \sum_i \int \frac{J_\nu}{h\nu} \exp[-\sigma_\nu N^a(\text{HI})] \sigma_\nu^i E_h(E^i, x) d\nu \quad , \quad (2)$$

where the summation is over species suffering primary ionization, and $E_h(E^i, x)$ is the energy deposited as heat by a primary electron originating from atomic species i with energy E^i in gas with electron fraction x . We used the results of Shull & van-Steenberg (1985) to compute E_h , and an updated version of the Morrison & McCammon (1983) results to compute σ_ν^i and σ_ν (McCammon 2003).

To compute the grain photoelectric heating rate due to FUV radiation we used the Weingartner & Draine (2001) expression

$$\Gamma_d = 10^{-26} \kappa G_0 f (G_0 \sqrt{T}/n_e, c_i) \exp(-\tau_\nu^d) \quad , \quad (3)$$

where Γ_d is in units of $\text{ergs s}^{-1} \text{H}^{-1}$, κ is the dust-to-gas ratio of the damped Ly α system relative to that of the ISM (ISM refers to the ISM of the Milky Way Galaxy), G_0 is $4\pi \int J_\nu d\nu$ integrated between 6 and 13.6 eV and is in units of $1.6 \times 10^{-3} \text{ergs s}^{-1} \text{cm}^{-2}$, f , which is proportional to the heating efficiency, is a function of $G_0 \sqrt{T}/n_e$ and the fitting constants, c_i (where $i=0 \rightarrow 6$), and τ_ν^d is the dust optical depth corresponding to N^a (H I).

Weingartner & Draine (2001) show that Γ_d is especially sensitive to two quantities: grain composition, i.e. the fraction of dust in silicate and carbonaceous grains, and the fraction of dust in small grains (radius $< 15 \text{\AA}$). Both are crucial because computations carried out so far show that small carbonaceous grains are the most efficient sources of photoelectric heating. The detection of the 2175 \AA absorption feature in two damped Ly α systems provide evidence for small carbonaceous grains at $z < 1$ (Junkkarinen et al. 2004; Motta et al. 2002), but the evidence is less clear for the redshift range of our sample. Pei, Fall, & Bechtold (1991) found no evidence for the 2175 \AA feature, yet detection was expected based on their reddening model. Thus damped Ly α systems with $z > 2$ could be comprised of silicate dust alone. However, all the published models for grain photoelectric heating include a population of small carbonaceous grains.

To address this problem we consider models with a range of heating efficiencies that should include that of silicate dust. We adopt a model in which the fraction of carbon locked in PAHs per H nucleus, $b_C=0$, and extinction ratio $R_V=3.1$, which is valid for the type of diffuse gas expected in damped Ly α systems (see Table 2, row 19 in Weingartner & Draine 2001); where $R_V \equiv A_V/E_{B-V}$, A_V is the visual extinction, and E_{B-V} is the color excess. We also assume a radiation spectrum approximating Draine’s (1978) fit to the interstellar radiation field in which case $G_0 \approx J_\nu / (10^{-19} \text{ergs cm}^{-2} \text{s}^{-1} \text{Hz}^{-1} \text{sr}^{-1})$ at $\lambda = 1500 \text{\AA}$ (see WPG). Application of this approximation to

background radiation involves no loss in generality since the background and interstellar radiation fields at $h\nu < h\nu_H$ arise from similar stellar populations (e.g. Bruzual & Charlot 2003). The resulting heating efficiency is the lowest predicted for the Weingartner & Draine (2001) models. The highest heating efficiency is predicted for their model with $R_V=3.1$, $b_C=6 \times 10^{-5}$, and an interstellar radiation spectrum (see their Table 2, last row). We shall examine the following three dust compositions: (1) a mix of silicate and carbonaceous grains in which $b_C=0$ and $R_V=3.1$, (2) a mix of silicate and carbonaceous grains in which $b_C=6 \times 10^{-5}$ and $R_V=3.1$, and (3) carbonaceous grains alone within the heating model of Bakes & Tielens (1994). In this way we shall test the sensitivity of our results to changes in grain properties. We show below that our results concerning the plausibility of background heating are independent of the properties of the grains, and depend only on the carbon abundance and assumptions about thermal equilibrium.

Next we use the WPG method for computing κ . Our prescription computes the fraction of Fe in grains and then assumes the number of depleted C or Si atoms per depleted Fe atom to be the same in damped Ly α systems as in the Galaxy ISM. The depletion of Fe is calculated from the ratio of the observed amount of Fe to an undepleted element: Zn or S would be ideal for this purpose. WPG use Si because (i) Si is measured over a wider range of redshifts than Zn, (ii) S is difficult to measure since the observed S II transitions occur frequently in the Ly α forest, and (iii) though Si is undoubtedly depleted, the observed depletion level is very low; i.e., $[\text{Si/S}] \approx 0$.² This does not lead to inconsistencies in the case of silicate dust because the computed values of κ are consistent with Si being depleted typically by less than 20 %.

WPG find $\kappa = 10^{[\text{Si/H}]_{\text{int}}} (10^{[\text{Fe/Si}]_{\text{int}}} - 10^{[\text{Fe/Si}]_{\text{gas}}})$ where $[\text{Si/H}]_{\text{int}}$ is the intrinsic abundance of Si relative to H, $[\text{Fe/Si}]_{\text{int}}$ is the intrinsic abundance of Fe relative to Si, and $[\text{Fe/Si}]_{\text{gas}}$ is the measured abundance of Fe relative to Si. Following WPG we assume minimal depletion occurs when $[\text{Fe/Si}]_{\text{int}} = -0.2$, i.e., an intrinsic enhancement of α elements such as Si, and maximum depletion occurs when $[\text{Fe/Si}]_{\text{int}} = 0$. Therefore, we adopt two Weingartner & Draine (2001) models, which should bracket a plausible range in heating rates. The “WD-low” model combines dust composition (1) with minimal depletion: this model is similar to one of the “SMC” models considered by WPG and results in the lowest heating rates.³ The “WD-high” model combines dust composition (2) with maximal depletion: this model produces the highest heating rates. For completeness we combine the Bakes & Tielens (1994) model of carbonaceous grains with the assumption of maximal depletion: this model, referred to as the “BT” model, produces heating rates between the predictions of the other two models, and is one of the “Gal” models considered by WPG. The properties of the models are summarized in Table 1.

The background mean intensities at redshift z , $J_\nu(z)$,²The abundance ratio of elements X and Y is given by $[\text{X/Y}] = \log_{10}(\text{X/Y}) - \log_{10}(\text{X/Y})_\odot$.

³Minimal depletion does not apply to damped Ly α systems in which $[\text{Fe/Si}]_{\text{gas}} > -0.2$. For these objects the “WD low” model is a hybrid of $b_C=0$ heating rates and maximal depletion.

TABLE 1
PARAMETERS FOR GRAIN HEATING MODELS

Name	[C/H] ^a	κ ^b	b_C ^c	R_V ^d	Reference ^e
WD-low	[Si/H]−0.2	f	0	3.1	(1)
WD-high	[Si/H]	g	6×10^{-5}	3.1	(1)
BT	[Si/H]	g	1.26×10^{-6}	...	(2)

^aCarbon abundance relative to solar.

^bdust-to-gas ratio relative to the Milky Way ISM

^cAbundance of C atoms per interstellar H nucleus in PAHs

^d $R_V \equiv A_V/E_{B-V}$, where A_V is visual extinction and E_{B-V} is the color excess.

^e(1) Weingartner & Draine 2001; (2) Bakes & Tielens 1994

$f 10^{[\text{Si/H}]} (10^{-0.2} - 10^{[\text{Fe/Si}]})$

$g 10^{[\text{Si/H}]} (1 - 10^{[\text{Fe/Si}]})$

were computed with the software package CUBA written and made available to us by Haardt & Madau (2003). These authors give a detailed description of how $J_\nu(z)$ is calculated from the luminosity function and spectra of QSOs and how the radiation is reprocessed by the intervening gas (Haardt & Madau 1996). Because grain photoelectric heating depends on J_ν at photon energies, $h\nu < h\nu_H$, where galaxies dominate QSOs, the galaxy contribution to the background radiation is crucial. For this reason we considered backgrounds that include the integrated contribution of galaxies. We used models in which the radiation escaping from the galaxies is attenuated by dust because this is the radiation that contributes to the background intensity incident on a given damped $\text{Ly}\alpha$ system. In this case the inferred luminosity per unit bandwidth per unit comoving volume decreases with redshift at $z > 1.5$, as found by Giavalisco et al. (2003). The predicted background spectra at the redshifts of five damped $\text{Ly}\alpha$ systems from our sample are shown in Figure 1. The factor of ~ 60 increase in J_ν as ν decreases across ν_H is the most striking feature in Figure 1. This feature is missing from backgrounds computed from QSOs alone (see Haardt & Madau 1996) and arises from stellar radiation, which is optically thick at the Lyman limit, and from an assumed escape fraction from galaxies of 10^{-1} at $h\nu \geq h\nu_H$ (Haardt & Madau 2003). Therefore, J_ν at $h\nu < h\nu_H$ is typically 10^{-20} ergs cm^{-2} s^{-1} Hz^{-1} sr^{-1} , which is a factor of ten higher than J_ν produced by QSOs alone. By comparison, the ambient FUV radiation in the ISM is characterized by $J_\nu \sim 10^{-19}$ ergs cm^{-2} s^{-1} Hz^{-1} sr^{-1} . The spectral regions that are critical for DLA heating correspond to $6 < h\nu < 13.6$ eV and $h\nu \gtrsim 400$ eV. Figure 1 shows that for a given dust-to-gas ratio and heating efficiency the FUV heating rates should decrease no more than 0.5 dex between $z=1.6$ and 4.3, while for a given $N(\text{H I})$ and metallicity the X-ray heating rates should increase by no more than 0.3 dex in the same range of redshifts.

2.2. Cooling

Cooling rates were computed according to the prescription given by W95 and WPG. Thus, we include cooling due to $\text{Ly}\alpha$ emission, and grain radiative recombination, which dominate at high temperatures, $T > 3000$ K. At lower temperatures, excitation of fine-structure states of abundant ions such as C^+ , O^0 , Si^+ , and Fe^+ , and excitation of metastable states of O^0 dominate the C II cooling rate. In all cases, $[\text{C II}]$ 158 μm emission, which arises through the transition between the $^2P_{3/2}$ and $^2P_{1/2}$ fine-structure states in the $2s^22p$ term of C^+ , is the dominant coolant in the CNM (cold-neutral medium) phase, while $\text{Ly}\alpha$ emission dominates in the WNM (warm-neutral medium) phase. Because CMB excitation of the $^2P_{3/2}$ state in C II increases with redshift, the spontaneous emission rate of 158 μm radiation per H atom, l_c , need not equal the cooling rate in low density gas at high redshifts. To separate the effects of cooling from radiative excitation we note that $l_c = n\Lambda_{\text{CII}} + (l_c)_{\text{CMB}}$, where $n\Lambda_{\text{CII}}$ is the cooling rate due to $[\text{C II}]$ 158 emission: the cooling rate is defined as the difference between collisional excitation and de-excitation rates of the $^2P_{3/2}$ state times the excitation energy, $h\nu_{ul}$, of the $^2P_{3/2} \rightarrow ^2P_{1/2}$ transition. The quantity $(l_c)_{\text{CMB}}$ is the spontaneous emission rate of

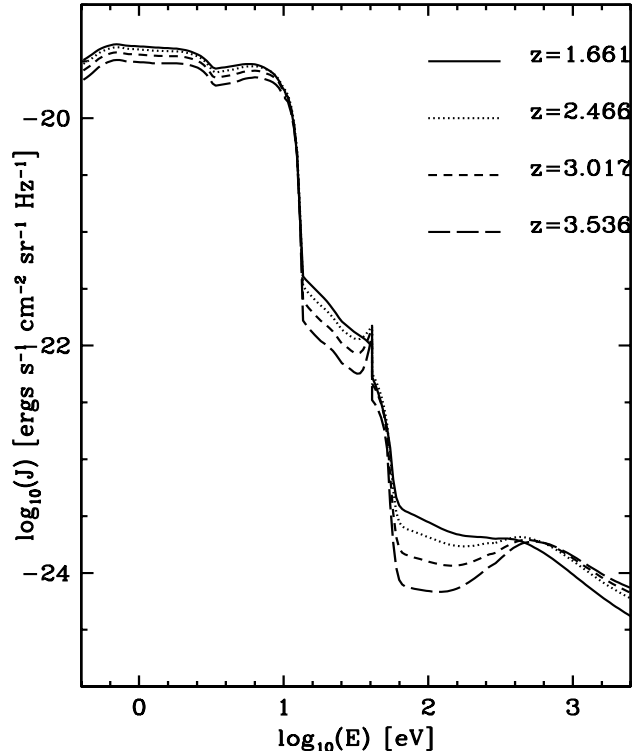


FIG. 1.— Haardt & Madau (2003) background spectra for damped $\text{Ly}\alpha$ systems with redshifts spanning the redshift interval of our sample. Spectral features are explained in the text

158 μm radiation per H atom in the limit of pure radiative excitation by the CMB, and equals $2(\text{C}/\text{H})A_{ul}h\nu_{ul} \exp\left[-h\nu_{ul}/[k(1+z)T_{\text{CMB}}]\right]$ where (C/H) is the carbon abundance. The quantity A_{ul} is the emission coefficient for spontaneous photon decay, and the current temperature of the CMB is $T_{\text{CMB}}=2.728$ K.

3. HEATING BY EXTERNAL BACKGROUND RADIATION

In this section we apply the formalism of § 2 to study the thermal structure of damped $\text{Ly}\alpha$ systems subject to external background radiation.

3.1. Background Heating of the $z = 1.919$ Damped $\text{Ly}\alpha$ System Toward Q2206–19

We tested the background heating hypothesis by comparing the predicted values of l_c with observations. The observed rate, $l_c^{\text{obs}} = N(\text{C II}^*)A_{ul}h\nu_{ul}/N(\text{H I})$ where $N(\text{C II}^*)$ is the observed column density of C II in the excited $^2P_{3/2}$ fine-structure state. The C II* column densities were derived from accurate measurements of C II* λ 1335.7 absorption lines arising from the $^2P_{3/2}$ state. WPG determined l_c^{obs} for 33 damped $\text{Ly}\alpha$ systems. Most of the data were acquired with the HIRES echelle spectrograph (Vogt et al. 1994) on the Keck I 10 m telescope, and in three objects with the UVES echelle spectrograph on the VLT 8 m telescope. More recently, l_c^{obs} was obtained by Prochaska et al. (2003) from measurements for 16 damped $\text{Ly}\alpha$ systems with the ESI echelle spectrograph imager (Sheinis et al. 2002) and with UVES for another system (Pettini et

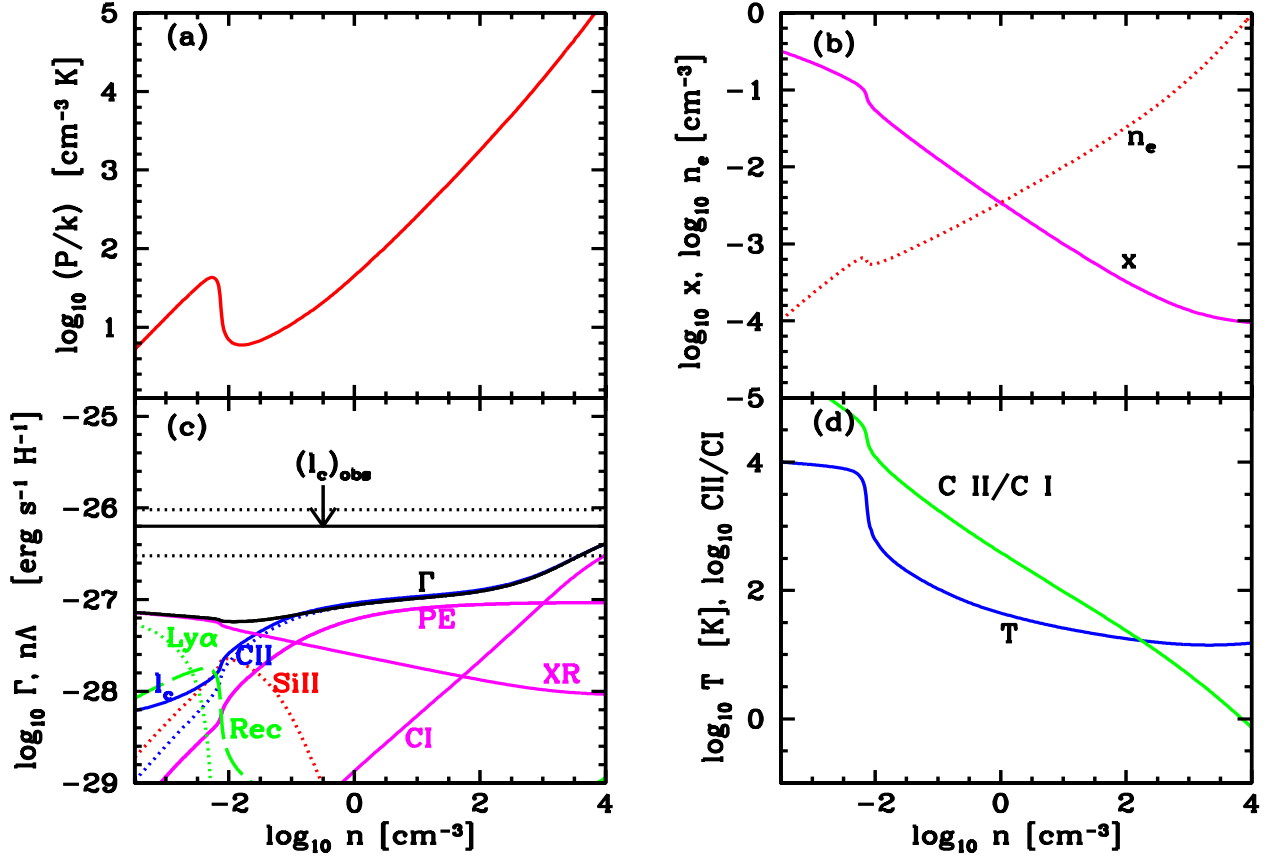


FIG. 2.— Two-phase diagrams for gas in the $z=1.919$ damped Ly α system toward Q2206–19. The heat input is FUV and soft X-ray background radiation. The heating mechanisms are grain photoelectric emission for FUV radiation and photoionization of H, He, and abundant elements for the X-rays. In this case we assume the “WD-low” model and minimal depletion (see text). The relevant data for this damped Ly α system are in Table 2. Panel (a) shows pressure versus density. Panel (b) shows fractional ionization, x , and electron density, n_e versus density. Magenta curves in panel (c) show grain photoelectric heating (PE), X-ray heating (XR), and C I photoionization heating rates versus density. Dotted blue curve is [C II] 158 μ m fine-structure cooling rate, and green curves are Ly α and grain recombination cooling rates. Dotted red curve is [S II] 35 μ m fine-structure cooling rate. Solid blue curve is [C II] 158 μ m spontaneous energy emission rate. Black curve (Γ) is total heating rate. Black horizontal solid line is $\log_{10} l_c^{obs}$ and black dotted horizontal lines are 2σ errors in $\log_{10} l_c^{obs}$. Panel (d) shows temperature and C II/C I ratio versus density.

al. 2002). Thus, the total sample consists of l_c^{obs} measurements for some 50 damped Ly α systems. In this paper we shall analyze the properties of 45 of these objects. These include 23 damped Ly α systems with positive detections of C II* absorption and 22 with upper limits on C II* absorption.

To predict l_c we computed thermal equilibria resulting from the energy balance condition, $\Gamma=n\Lambda$. The total heating rate $\Gamma=\Gamma_{XR}+\Gamma_d$, where the radiation input is from XR and FUV background radiation alone; i.e., no internal heat sources are included. The quantities n and Λ are gas volume density of hydrogen and total cooling function respectively. Thermal equilibrium constrains the temperature, pressure, cooling rates, etc. to be unique functions of density. It also results in l_c as a unique function of density, i.e., $l_c(n)$.

In order to interpret the results for our full sample of 45 damped Ly α systems the reader is referred to Figure 2 for the phase diagrams of the $z = 1.919$ damped Ly α system toward Q2206–19, one of our sample damped Ly α systems, which is hereafter referred to as the Q2206A damped

Ly α system. The figure shows equilibrium curves for (a) pressure, (b) electron fraction and electron density, (c) cooling rates, heating rates, and l_c , and (d) temperature and C II/C I column-density ratios (hereafter C II/C I denotes the ratio $N(\text{C II})/N(\text{C I})$) as functions of hydrogen density. The equilibria are computed for the “WD-low” model. The curves show the classical two-phase equilibria (see Field, Goldsmith, & Habing 1969; W95) exhibited by neutral gas layers heated by the grain photoelectric mechanism and ionized by soft X-rays (W95, WPG). In that case the equilibria admit the presence of a thermally stable WNM at low densities and high temperatures separated from a thermally stable CNM at high densities and low temperatures by a thermally unstable intermediate-density region in which $\partial(\log P)/\partial(\log n) < 0$.⁴ Figure 2c shows $n\Lambda_{CII}$ (dotted blue curve) to increase with density.

⁴The thermally unstable region occurs at lower densities than in the ISM of the Galaxy because the FUV heating rate produced by external background radiation incident on gas with a low dust-to-gas ratio is about 100 times lower than in the ISM where the heat source is internal FUV radiation emitted by stars in the Galaxy (see WPG).

The increase is steep at $n < 10^{-2} \text{ cm}^{-3}$, very steep at $n \approx 10^{-2} \text{ cm}^{-3}$, flatter at $10^{-2} < n < 10^{-1} \text{ cm}^{-3}$, insensitive to n at $10^{-1} < n < 10^{+2} \text{ cm}^{-3}$, and steeper again at $n > 10^{+2} \text{ cm}^{-3}$.

To understand this behavior we note that the cooling rate is dominated by processes other than $158 \mu\text{m}$ emission at $n < 10^{-1} \text{ cm}^{-3}$. Consequently, $n\Lambda_{\text{CII}}$ does not track the total heating rate, Γ , which is flat at the latter densities. The explicit form of $n\Lambda_{\text{CII}}$ under these conditions is given by

$$n\Lambda_{\text{CII}} \propto n_e(\text{C}/\text{H})\Omega(^2P_{3/2}, ^2P_{1/2})T^{-1/2}\exp(-h\nu_{ul}/kT) \quad , \quad (4)$$

where the collision strength, $\Omega(^2P_{3/2}, ^2P_{1/2})$, is relatively insensitive to changes in n and T (see Blum & Pradhan 1992). At $n < 10^{-2} \text{ cm}^{-3}$ the increase in $n\Lambda_{\text{CII}}$ is driven primarily by the increase in electron density with increasing n (see Figure 2b) because (1) the Boltzmann factor, $\exp(-h\nu_{ul}/kT)$, is constant since $T \gg h\nu_{ul}/k = 92 \text{ K}$, and (2) T is insensitive to n at these densities (see Figure 2d). At $n \approx 10^{-2} \text{ cm}^{-3}$ the very steep drop in T marks the transition between WNM and CNM gas in the region of thermal instability due to the shift from Ly α cooling to fine-structure line cooling by low ions of abundant elements. The sharp increase in $n\Lambda_{\text{CII}}$ is due to the increase in the $T^{-1/2}$ factor because at these temperatures the Boltzmann factor is constant. The decrease in T also increases the radiative recombination coefficients, which cause the abrupt drops seen in x , n_e , and C II/C I. When $10^{-2} < n < 10^{-1} \text{ cm}^{-3}$ the increase in $n\Lambda_{\text{CII}}$ is modulated by the Boltzmann factor which decreases as T becomes comparable to $h\nu_{ul}/k$. However, at $n > 10^{-1} \text{ cm}^{-3}$ the dependence of $n\Lambda_{\text{CII}}$ on n is dictated by the density dependence of the total heating rate, $\Gamma(n)$, since $n\Lambda_{\text{CII}}$ dominates the cooling rate at these densities and thus equals the total heating rate. This accounts for the flat behavior of $n\Lambda_{\text{CII}}$ at $10^{-1} < n < 10^{+2} \text{ cm}^{-3}$ where the grain photoelectric heating rate dominates and is independent of density, and the steep increase of $n\Lambda_{\text{CII}}$ at $n > 10^2 \text{ cm}^{-3}$ where the C I photoionization heating rate per atom becomes dominant. Note that $l_c(n)$ departs from $n\Lambda_{\text{CII}}$ only at $n < 10^{-2} \text{ cm}^{-3}$ where radiative excitations by CMB radiation dominate collisional excitations.

Comparison between predicted and observed values of l_c in the case of the Q2206A damped Ly α system shows that heating and ionization by background radiation cannot account for the observed $158 \mu\text{m}$ cooling rate unless the densities are higher than $n > 10^{3.4} \text{ cm}^{-3}$ for the “WD-low” model shown in Figure 2 (specifically see Figure 2c). But in the case of FUV background heating alone, densities this large are ruled out by the observational constraint, C II/C I $> 2 \times 10^4$. The connection between n and C II/C I follows from the condition of photoionization equilibrium, which implies

$$\frac{\text{C II}}{\text{C I}} \propto \frac{G_0}{\alpha(\text{CI})xn} \quad , \quad (5)$$

where $\alpha(\text{CI})$ is the C I radiative recombination coefficient. In thermal equilibrium C II/C I and x are functions of n , which are plotted in Figure 2. The low value of G_0 ($=0.14$) and the large lower limit on C II/C I combine to set an upper limit on density, $n < 10^{-2} \text{ cm}^{-3}$ for FUV background heating alone. From the $l_c(n)$ curve in Figure

2c we see this corresponds to $l_c < 10^{-27.8} \text{ ergs s}^{-1} \text{ H}^{-1}$ which should be compared to $l_c^{\text{obs}} > 10^{-26.5} \text{ ergs s}^{-1} \text{ H}^{-1}$; i.e., the $2\text{-}\sigma$ lower limit denoted by the lower dotted horizontal line. This demonstrates that background heating alone cannot account for the value of l_c^{obs} .

Although this discrepancy was derived for the “WD-low” grain model, it is quite general as it is insensitive to grain composition. To see this we compare $l_c(n)$ with l_c^{obs} for all 45 damped Ly α systems in Table 2. In each damped Ly α system we compare the predictions of the “WD-low” model with the “WD-high” and “BT” models. Before discussing the full sample we focus first on the Q2206A damped Ly α system. Figure 3a (first column and second row from the top) shows the $l_c(n)$ predicted by each model is more than a factor of 10 below the lower limit on l_c^{obs} at densities, $n < 10^{-2} \text{ cm}^{-3}$, permitted by the C II/C I constraint. The discrepancies between $l_c(n)$ and l_c^{obs} differ slightly for each model for reasons that are independent of grain properties. First, notice that at $n < 10^{-2} \text{ cm}^{-3}$ the $l_c(n)$ predicted by the “WD-high” and “BT” models are degenerate and higher than predicted by the “WD-low” model. At such low densities the gas is a WNM where $l_c(n) \propto n_e(\text{C}/\text{H})$. Because there are no unsaturated transitions of C II we assume C traces Fe and as a result we let $[\text{C}/\text{H}] = [\text{Si}/\text{H}] + [\text{Fe}/\text{Si}]_{\text{int}}$ to determine the carbon abundance (see § 5.1 in WPG). From Table 1 we see that the carbon abundance, $[\text{C}/\text{H}]$, is lower in the “WD-low” model than in the “WD-high” or “BT” models because $[\text{Fe}/\text{Si}]_{\text{int}} = -0.2$ for the minimal depletion assumed in the “WD-low” model and $[\text{Fe}/\text{Si}]_{\text{int}} = 0$ for the maximal depletion assumed in the “WD-high” and “BT” models. Therefore, $l_c(n)$ is predicted to be lower in the “WD-low” model. Second, the C II/C I constraints on $l_c(n)$ will differ because the observational limits on C II/C I will be lower by 0.2 dex in the “WD-low” model. This is because $N(\text{C II})$ will be 0.2 dex lower while $N(\text{C I})$ will be the same, as it is inferred directly from the strength of C I $\lambda 1656.9$ absorption. The predicted dependence of C II/C I on n will also differ in each model because the $T(n)$ and $n_e(n)$ relations differ. The important point is that the C II/C I limits restrict gas heated by background radiation to the WNM phase where the limits on $l_c(n)$ depend only on the carbon abundance and the assumption of thermal equilibrium, both of which are independent of grain properties. This is a generic trait of the full sample to which we now turn.

3.2. Background Heating of the Full Sample

We repeated these procedures for the 44 remaining damped Ly α systems for which it was possible to calculate thermal equilibria for all three dust models. This yielded phase diagrams for a total of 23 damped Ly α systems in which C II* $\lambda 1335.7$ was detected and 22 with upper limits. Comparisons between l_c^{obs} and the predicted $l_c(n)$ curves are plotted for the detections in Figures 3a and 3b, and for the upper limits in Figures 4a and 4b. Relevant data for all of the damped Ly α systems are given in Table 2. The coordinate name of the background QSO is given in column 1, the absorption redshift in column 2, the value of $\log_{10} \text{C II/C I}$ in column 3, the observed $[\text{Fe}/\text{H}]$ and $[\text{Si}/\text{H}]$ abundance ratios in columns 4 and 5, $\log_{10} l_c^{\text{obs}}$ in column 6, and the mean intensity due to starlight, J_{ν}^{stars} , in column

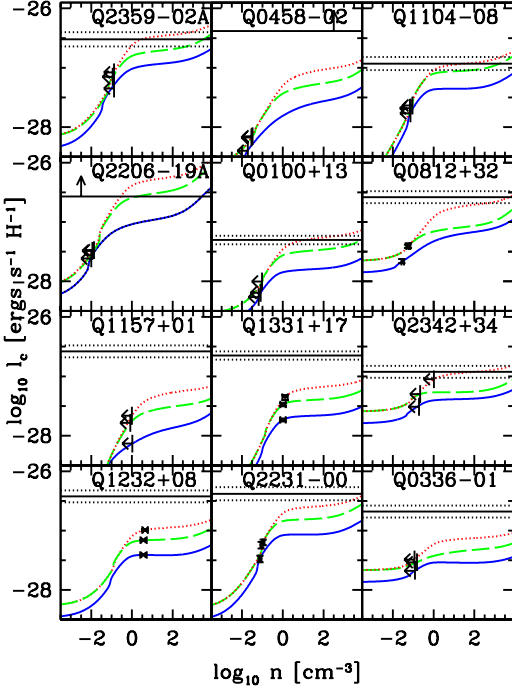


FIG. 3.— $l_c(n)$ curves for 12 damped Ly α systems with positive detections of C II* $\lambda 1335.7$ absorption. The $l_c(n)$ are computed from thermal equilibria where heat input is from background radiation alone. Solid curves show $l_c(n)$ for the “WD-low” model, dashed curves for the “BT” model, and dotted curves for the “WD-high” model. In all cases the heating mechanisms are grain photoelectric heating and X-ray photoionization. Data are shown as solid horizontal lines for $\log_{10} l_c^{obs}$ and dotted lines for $1-\sigma$ errors in $\log_{10} l_c^{obs}$. The solid horizontal lines in Q2206–19 and Q0458–02 damped Ly α systems represent $2-\sigma$ lower limits on $\log_{10} l_c^{obs}$. Arrows on $l_c(n)$ curves are upper limits on n imposed by observed lower limit on C II/C I. These become data points and error bars for Q1232+08, Q1331+17, Q2231–00, and Q0812+32 where C II/C I is measured.

7 (see § 5).

In Figures 3a and 3b we compare the predicted $l_c(n)$ with l_c^{obs} for damped Ly α systems with positive detections. In every case in Figure 3a and in 9 out of 12 cases in Figure 3b the predictions fall significantly (more than $4\sigma_{\log_{10} l_c}$) below the observations at densities permitted by the C II/C I ratios (shown as horizontal arrows directed toward decreasing n). Most of the predicted $l_c(n)$ curves exhibit behavior similar to that described for the Q2206A damped Ly α system. Specifically, the “WD-high” and “BT” models are degenerate at low n , but diverge at n sufficiently large that $l_c(n)$ equals the grain photoelectric heating rate. At the latter densities $l_c(n)$ is higher for the “WD-high” model than the “BT” model because of the difference in heating efficiencies. Furthermore, $l_c(n)$ for both “WD-high” and “BT” models are higher than for the “WD-low” models because the heating efficiencies and κ (Table 1) are higher in the “WD-high” and “BT” models. However, there are differences with the Q2206A result. First Figure 3b shows that in some damped Ly α systems with very low dust-to-gas ratios (e.g. Q0953+47 and Q0747+27) $l_c(n)$ decreases rather than increases with n above densities corresponding to the WNM–CNM transition zone. This behavior stems from the low values of κ , which suppress grain photo-electric heating in favor of

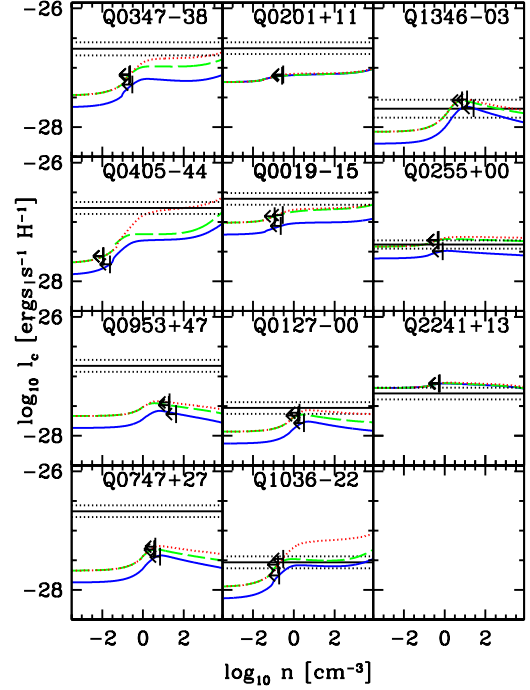


Fig3b

X-ray heating, which decreases with n (see Figure 2c). Second, $l_c(n)$ exhibits a flat plateau at low densities in damped Ly α systems with large redshifts since $l_c(n)$ approaches $(l_c)_{CMB}$ in the low density limit. Because $(l_c)_{CMB} \ll l_c^{obs}$, the CMB has only marginal effect on the [C II] $158 \mu\text{m}$ emission rate for every damped Ly α system in Figure 3a and most damped Ly α systems in Figure 3b.

On the other hand, background radiation is the likely source of $(l_c)_{obs}$ for two of the 11 positive detections in Figure 3b. Specifically, the CMB is the dominant factor for the Q0255+00 and Q2241+13 damped Ly α systems where $(l_c)_{CMB} \approx (l_c)_{obs}$. It accounts for l_c^{obs} at all densities in all three grain models for Q2241+13⁵, and it accounts for l_c^{obs} in the “WD-high” and “BT” models for Q0255+00. But since the “WD-low” model predicts $l_c(n)$ to be $2.6\sigma_{\log_{10} l_c}$ below l_c^{obs} at low n , a heat source in addition to background radiation may be required for the latter damped Ly α system. The CMB is unlikely to explain l_c^{obs} for any of the remaining damped Ly α systems with positive detections of C II* absorption. Therefore, with one exception we find that $\log_{10} l_c^{obs} - \log_{10} l_c(n) \geq 3\sigma_{\log_{10} l_c}$ at densities permitted by the C II/C I constraint when $l_c(n)$ is calculated under the assumption that external background radiation is the sole source of heating. The exception is the Q1346–03 damped Ly α system (see Figure 3b) in which heating by X-ray background radiation can account for l_c^{obs} when $1 < n < 25 \text{ cm}^{-3}$. Therefore, we conclude that background radiation alone cannot explain

⁵The “WD-low” model for the Q2241+13 damped Ly α system is degenerate with the “WD-high” and “BT” models in Figure 3b since we assumed maximal rather than minimal depletion. This occurs because $[\text{Fe}/\text{Si}]_{gas} > -0.2$ in this and in the Q0201+11, Q1021+30, Q1506+52, and Q2344+12 damped Ly α systems.

TABLE 2
 DLA PROPERTY

QSO	z_{abs}	$\log_{10}(C\ II/C\ I)^c$	[Fe/H]	[Si/H]	$\log_{10} l_c$	G_0^f
(1)	(2)	(3)	(4)	(5)	erg s $^{-1}$ H $^{-1}$	(7)
Q0019-15 ^a	3.439	>3.44	-1.59±0.11	-1.06±0.11	-26.61±0.10	6.8
Q0100+13 ^a	2.309	>4.14	-1.90±0.09	-1.46±0.08	-27.30±0.07	2.4
Q0127-00 ^b	3.727	>2.87	-2.60±0.09	-2.18±0.23	-27.53±0.12	1.5 (21.8)
Q0133+04A ^b	3.773	>3.38	-0.90±0.10	-0.64±0.10	< -25.92
Q0133+04B ^b	3.692	>2.30	-2.69±0.10	-2.00±0.20	< -27.66
Q0149+33 ^a	2.141	>2.80	-1.77±0.10	-1.49±0.11	< -27.24
Q0201+11 ^a	3.387	>3.22	-1.41±0.11	-1.25±0.15	-26.67±0.14	5.4
Q0209+52 ^b	3.864	>1.71	-2.89±0.20	-2.65±0.10	< -27.12
Q0255+00 ^a	3.915	>3.23	-2.05±0.10	-1.78±0.05	-27.38±0.07	1.1 (17.3)
Q0307-49 ^a	4.466	>2.79	-1.96±0.22	-1.55±0.12	< -26.60
Q0336-01 ^a	3.062	>3.86	-1.80±0.11	-1.41±0.10	-26.68±0.10	12.2
Q0347-38 ^a	3.025	>3.33	-1.62±0.08	-1.17±0.03	-26.68±0.03	6.8
Q0405-44 ^b	2.595	> 4.58	-1.33±0.11	-0.96±0.19	-26.76±0.10	6.1
Q0458-02 ^a	2.039	> 4.60	-1.77±0.10	-1.19±0.09	> -26.38	>19.1
Q0741+47 ^a	3.017	>2.85	-1.93±0.10	-1.69±0.10	< -27.45
Q0747+27 ^b	3.900	>2.44	-2.53±0.10	-2.03±0.10	-26.67±0.14	17.3
Q0812+32 ^b	2.626	4.07±0.10	-1.74±0.10	-0.96±0.10	-26.58±0.10	9.4
Q0836+11 ^a	2.465	>3.31	-1.40±0.10	-1.15±0.11	< -26.98
Q0953+47 ^b	4.244	>1.96	-2.50±0.17	-2.23±0.15	-26.82±0.21	17.3
Q1021+30 ^b	2.949	>2.35	-2.32±0.12	-2.17±0.10	< -27.31
Q1036-22 ^b	2.773	>3.65	-1.82±0.10	-1.41±0.10	-27.65±0.14	(12.2)
Q1104-18 ^a	1.661	>3.87	-1.48±0.10	-1.04±0.10	-26.88±0.11	4.3
Q1108+22 ^a	3.608	>2.70	-2.12±0.10	-1.80±0.11	< -27.68
Q1132+22 ^b	2.783	>2.95	-2.48±0.10	-2.07±0.16	< -27.59
Q1157+01 ^b	1.944	>3.34	-1.81±0.11	-1.37±0.12	-26.58±0.13	15.3
Q1202-07 ^a	4.383 ^e	-2.19±0.19	-1.81±0.14	< -27.06
Q1215+33 ^a	1.999	>3.53	-1.70±0.09	-1.48±0.07	< -27.30
Q1223+17 ^a	2.466	>4.07	-1.84±0.10	-1.59±0.10	< -27.02
Q1232+08 ^a	2.337	2.41±0.10	-1.72±0.13	-1.22±0.15	-26.42±0.14	17.1
Q1331+17 ^a	1.776	2.93±0.10	-2.06±0.41	-1.45±0.04	-26.65±0.07	10.8
Q1337+11 ^b	2.795	>2.59	-2.39±0.10	-1.79±0.15	< -27.38
Q1346-03 ^a	3.736	>2.13	-2.63±0.10	-2.33±0.10	-27.69±0.15	0.35 (15.4)
Q1354-17 ^b	2.780	>1.82	-2.43±0.17	-1.88±0.16	< -26.99
Q1506+52 ^b	3.224	>2.13	-2.46±0.10	-2.30±0.15	< -27.30
Q1946+76 ^a	2.884	>2.83	-2.53±0.06	-2.23±0.06	< -27.33
Q2206-19A ^a	1.919	>4.48	-0.86±0.06	-0.42±0.07	-26.20 ^{+0.18} _{-0.32} ^d	22.8
Q2206-19B ^b	2.076	>2.22	-2.61±0.06	-2.31±0.07	< -26.80
Q2231-06 ^b	2.066	3.58±0.10	-1.40±0.12	-0.88±0.10	-26.38±0.11	13.4
Q2237-06 ^a	4.080 ^e	-2.14±0.17	-1.87±0.11	< -27.51
Q2241+13 ^b	4.282	>3.07	-1.90±0.11	-1.78±0.11	-27.29±0.14
Q2334-09 ^b	3.057	>3.29	-1.63±0.10	-1.15±0.12	< -27.04
Q2342+34 ^b	2.908	>3.59	-1.62±0.12	-1.19±0.11	-26.92±0.13	4.3
Q2344+12 ^b	2.538	>2.41	-1.83±0.11	-1.74±0.12	< -26.93
Q2348-14 ^a	2.279	>3.09	-2.24±0.08	-1.92±0.08	-26.88±0.12	10.9
Q2359-02A ^a	2.095	>3.52	-1.66±0.10	-0.78±0.10	-26.52±0.12	8.2

^aData from WPG

^bData presented here for the first time

^cEstimates derived assuming $[C/H]=[Si/H]$, which is appropriate for the “WD-high” and “BT” model. Estimates for the “WD-low” models are 0.2 dex lower (see Table 1)

^dIn this case errors are $2-\sigma$

^eWavelength regions covering C I transitions not observed

^fEntries are CNM solutions for J_{ν}^{stars} (in units of 10^{-19} ergs cm $^{-2}$ s $^{-1}$ Hz $^{-1}$ sr $^{-1}$) in damped Ly α systems with positive detections. Numbers in parentheses denote WNM solutions for cases where WNM hypothesis is plausible.

the inferred 158 μ m emission in 20 out of the 23 positive detections in Figures 3a and 3b. In each of the 20 cases an internal source of heating is required.

Figures 4a and 4b show $l_c(n)$ curves predicted for the 22 damped Ly α systems with upper limits on l_c^{obs} . As for the damped Ly α systems with positive detections, l_c^{obs} exceeds $l_c(n)$ in most cases. But there is an important difference: since l_c^{obs} in Figures 4a and 4b are upper limits, the discrepancy with the model predictions need not require the presence of internal heat sources. Thus, if the true l_c^{obs} revealed by future detections of C II* absorption intersected the $l_c(n)$ curves, then background heating could account for the C II cooling rates, provided the gas density satisfied the condition $l_c(n)=l_c^{obs}$, which defines the density $n=n_{BKD}$. Because n_{BKD} lies in the WNM phase for every damped Ly α system shown in Figure 4, the gas would be a WNM. Most of the damped Ly α systems illustrated in Figure 4 are candidates for this condition since the upper limits on l_c^{obs} are typically less than 0.2 dex above $l_c(n)$. But, internal heating would be required if the true l_c^{obs}

remain above the $l_c(n)$ curves for all n . This is clearly possible for the damped Ly α systems toward Q1223+17, Q2348-14, Q2206-19A, and Q0209+52 where the upper limits on l_c^{obs} are typically more than 0.5 dex above the peaks in the $l_c(n)$ curves. In § 5.2 we show that internal heating may also be present even when l_c^{obs} dips below the peaks of the $l_c(n)$ curves, which we emphasize are predicted for the case of background heating alone.

To summarize, the evidence discussed so far suggests the following: Most damped Ly α systems with positive detections of C II* absorption require internal heat sources, and we are able to rule out the hypothesis that damped Ly α systems with upper limits on C II* absorption consist of CNM gas heated by background radiation alone. In § 4 we discuss independent evidence for internal heating by starlight for one damped Ly α system in which C II* absorption is detected. In § 5 we consider this possibility for all the damped Ly α systems in Table 2, including those with upper limits on C II* absorption.

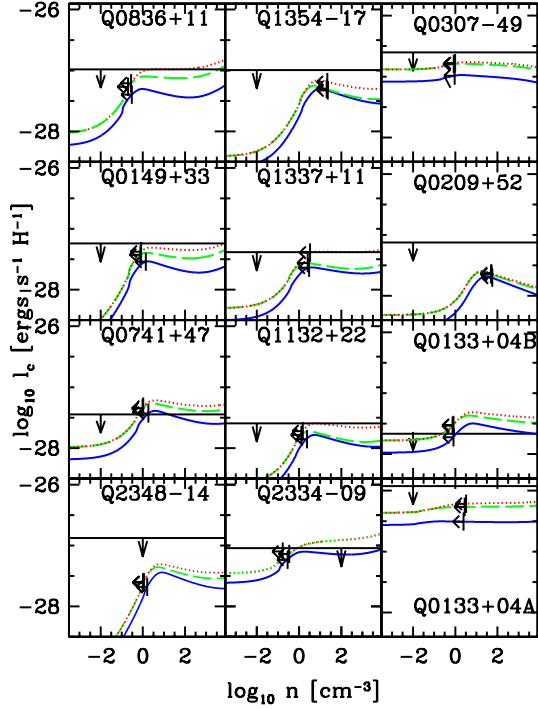


FIG. 4.— $l_c(n)$ curves for 12 damped Ly α systems with upper limits on C II* λ 1335.7 absorption. The $l_c(n)$ curves are computed as in Figures 3a and 3b. Resulting 2- σ upper limits on $\log_{10} l_c^{obs}$ are solid horizontal lines with downward pointing arrows.

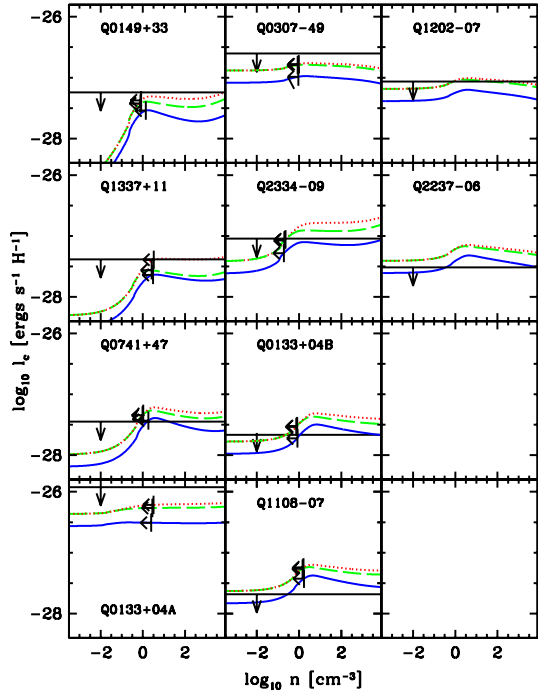


Fig4b

4. INDEPENDENT EVIDENCE FOR HEATING BY STARLIGHT IN A DAMPED Ly α SYSTEM

In § 3.2 we concluded that heating by external background radiation is insufficient to account for the [C II] 158 μ m emission rates inferred for most damped Ly α systems with detected C II* λ 1335.7 absorption. Rather, an internal heat source is required. WPG and WGP suggested grain photoelectric heating by FUV radiation from stars associated with the absorbing gas as the heat source. They neglected background radiation because the computed radiation fields available to them included the contribution by QSOs alone (e.g. Haardt & Madau 1996). These fields have a factor of 10 lower intensity than the galaxy contribution at $h\nu < h\nu_H$ and, therefore, make an insignificant contribution to the required heating rate.

Evidence supporting grain photoelectric heating was presented in WGP. In particular the statistically significant correlation between l_c^{obs} and dust-to-gas ratio, κ , argues against mechanical heating mechanisms such as turbulent dissipation (e.g. Wolfire et al. 2003) and is instead strong evidence for grain photoelectric heating, provided l_c^{obs} represents the heating rate. Accurate upper limits on Si II* λ 1264.7 absorption established by Howk et al. (2004a,b) for three damped Ly α systems with detected C II* λ 1335.7 absorption give independent evidence that the C II* absorption arises in CNM gas and, as a result, l_c^{obs} must equal the heating rate (see § 3.1). Therefore, the evidence accumulated so far indicates (1) photoejection of electrons from grains as the heating mechanism, and (2) that background radiation does not provide sufficient photons. While this points toward locally produced FUV radiation, i.e. starlight, as the source of photons, WGP did not offer direct evidence for a link between the inferred radiation intensity and starlight in a given damped Ly α system.

In this section we present evidence for such a link. Specifically, Møller et al. (2002) detected starlight emitted by a galaxy associated with the Q2206A damped Ly α system. Therefore, it is possible to deduce J_ν directly and compare it with the J_ν inferred from

C II* absorption at $h\nu = 8$ eV. That is the purpose of this section.

4.1. J_ν^{stars} Inferred From C II* Absorption

Figure 5a shows the C II* λ 1335.7 absorption profile for the Q2206A damped Ly α system. This spectrum was acquired with UVES, the echelle spectrograph on the VLT 8 m telescope, by Pettini et al. (2002) and was obtained by us from the UVES archive. This transition is clearly detected between $v = -20$ and $v = +30$ km s $^{-1}$. At $v > +30$ km s $^{-1}$ the C II* transition is blended with a broad Ly α forest feature extending between $v = +30$ and $v = +300$ km s $^{-1}$. If one assumes that C II* λ 1335.7 cuts off at $v = +30$ km s $^{-1}$, then $\log_{10} N(\text{C II}^*) = 13.65 \pm 0.05$ cm $^{-2}$. This is the column density used to compute l_c^{obs} in Figure 3. However, this is likely to be a lower limit to the actual column density. The reasons are illustrated in Figures 5b and 5c, which show the Si II λ 1808.0 and Ni II λ 1370.1 velocity profiles (Prochaska & Wolfe 1997a). These and all other low-ion resonance-line profiles in this damped Ly α system exhibit significant absorption between $v = -20$ and $v = +120$ km s $^{-1}$. In fact Prochaska & Wolfe (1997b) used

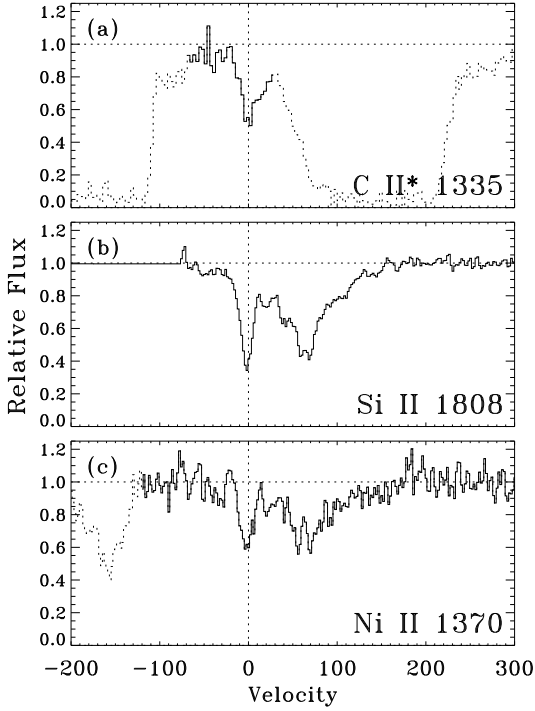


FIG. 5.— Panel (a) shows velocity profile of C II* λ 1335.7 absorption (solid curve) in the Q2206A damped Ly α system. Dotted curve at lower velocities is C II λ 1334.5 absorption. Dotted curve at higher velocities is a Ly α forest line. Data acquired with UVES on the VLT. Panels (b) and (c) shows Si II λ 1808.0 and Ni II λ 1370.1 velocity profiles in the same absorption system. Data acquired by Prochaska & Wolfe (1997a). Vertical line shows coincidence of the lowest velocity component in all three transitions.

the low-ion profiles to obtain an absorption velocity interval, $\Delta v = 130 \text{ km s}^{-1}$ for the Q2206A damped Ly α system. The C II* profile is likely to exhibit a similar velocity structure since the C II* and low-ion resonance-line velocity profiles are indistinguishable in all but one damped Ly α system for which C II* λ 1335.7 is detected (see WGP). When we integrate the Si II and Ni II profiles over the entire absorption range, we find the column densities to be 0.50 dex higher than when integrated from $v = -20$ to $+30 \text{ km s}^{-1}$. Correcting the C II* column density by this factor we find $\log_{10} N(\text{C II}^*) = 14.15 \pm 0.10 \text{ cm}^{-2}$. We take the latter value as an upper limit on $N(\text{C II}^*)$ and $\log_{10} N(\text{C II}^*) = 13.65 \text{ cm}^{-2}$ for the lower limit. By adopting the mean of these for the detected value, we find $\log_{10} N(\text{C II}^*) = 13.97^{+0.18}_{-0.32}$ where the errors are the differences between the limits and the mean. The corresponding $158 \mu\text{m}$ emission rates are given by $\log_{10} l_c^{obs} = -26.20^{+0.18}_{-0.32} \text{ ergs s}^{-1} \text{ H}^{-1}$. We believe the errors in $\log_{10} N(\text{C II}^*)$ and $\log_{10} l_c^{obs}$ correspond to 95% confidence intervals.

To obtain the FUV mean intensity generated by local stars from l_c^{obs} we recompute the thermal equilibrium of the neutral gas. First we compute the grain photoelectric heating rate, Γ_d , due to the total mean intensity, $J_\nu = J_\nu^{stars} + J_\nu^{bkd}$, where J_ν^{stars} and J_ν^{bkd} are the FUV intensities due to local stars and background radiation. Then we recompute the X-ray heating rate by adding the contribution from hot gas assumed to be associated with local stars to the X-ray background intensity (see Wolfire et al. 1995 and WGP). We also include heating by cos-

mic rays generated by local stars. In both cases we let the heating rates be proportional to the source function for J_ν^{stars} ; i.e., the SFR per unit area, ψ_* (see WPG). We compute the total heating rates for a grid of mean intensities⁶ in the range $5 \times 10^{-21} < J_\nu^{stars} < 5 \times 10^{-17} \text{ ergs cm}^{-2} \text{ s}^{-1} \text{ Hz}^{-1} \text{ sr}^{-1}$. We use the prescription discussed in § 2 to obtain metal abundances and dust-to-gas ratios, which are used to generate cooling rates and heating rates respectively. Thermal equilibrium models give $P(n)$ and $l_c(n)$ curves similar to those shown in Figure 2. To obtain J_ν^{stars} corresponding to a given l_c^{obs} we assume damped Ly α systems to be two-phase media in which CNM gas is in pressure equilibrium with WNM gas at pressure $P_{eq} = (P_{min} P_{max})^{1/2}$, where P_{min} and P_{max} are the pressure minimum and maximum exhibited by a two-phase medium in thermal equilibrium (see Figure 2a). This results in two unique solutions for each l_c^{obs} , one in which C II* absorption arises in the CNM and the other in the WNM. In WGP we argued against the WNM hypothesis as it gives rise to more background radiation than observed at the current epoch. The argument against the WNM hypothesis is further supported by the absence of Si II* λ 1264.7 absorption in three damped Ly α systems (see Howk et al. 2004a,b). Nevertheless, we consider the WNM solutions anew since they provide independent tests of the WNM hypothesis.

Figure 6 shows the Q2206A phase diagrams corresponding to the CNM solution. In this case the mean intensity resulting in $l_c(n) = l_c^{obs}$ at the CNM density, n_{CNM} , is given by $J_\nu^{stars} = 2.3 \times 10^{-18} \text{ ergs cm}^{-2} \text{ s}^{-1} \text{ Hz}^{-1} \text{ sr}^{-1}$, where n_{CNM} is the higher density root of the polynomial, $P(n) - P_{eq} = 0$. We find $n_{\text{CNM}} = 1.3 \text{ cm}^{-3}$ as shown by the vertical dot-dashed line which crosses the intersections between $l_c(n)$ with l_c^{obs} and $P(n)$ with P_{eq} (Figures 6a and 6c). We again adopt the “WD-low” model.

Comparison between Figures 2 and 6 reveal several differences. First, P_{max} and P_{min} occur at higher densities when local radiation fields with intensities much higher than the background are included. These pressures occur where fine-structure cooling dominates resonance line cooling and signify the transition from WNM to CNM gas. In the CNM gas the temperature is determined by the balance between [C II] $158 \mu\text{m}$ cooling and grain photoelectric heating in the low temperature limit. Because the density threshold above which grain photoelectric heating dominates X-ray and cosmic ray heating is proportional to J_ν^{stars} , the transition to CNM occurs at higher densities as J_ν^{stars} increases (compare Figures 2c and 6c). The larger value of J_ν also results in larger C II/C I ratios at a given n (compare Figures 2d and 6d). Therefore, the high density solutions ruled out for background heating alone are allowed when local sources are included. Indeed the value of n_{CNM} is consistent with the lower limit set on C II/C I for this damped Ly α system.

To make realistic predictions of J_ν^{stars} for the “WD-low” model we proceeded as follows. First, we computed J_ν^{stars} corresponding to l_c^{obs} . We repeated the calcula-

⁶In WGP we generated the J_ν grid starting with a grid of $\log_{10} \psi_*$ between -4.0 and $0.0 \text{ M}_\odot \text{ yr}^{-1} \text{ kpc}^{-2}$. In this paper, we work with J_ν directly since it can be inferred from observations. We consider the SFRs later in § 6 when we connect J_ν^{stars} to the rate of star formation.

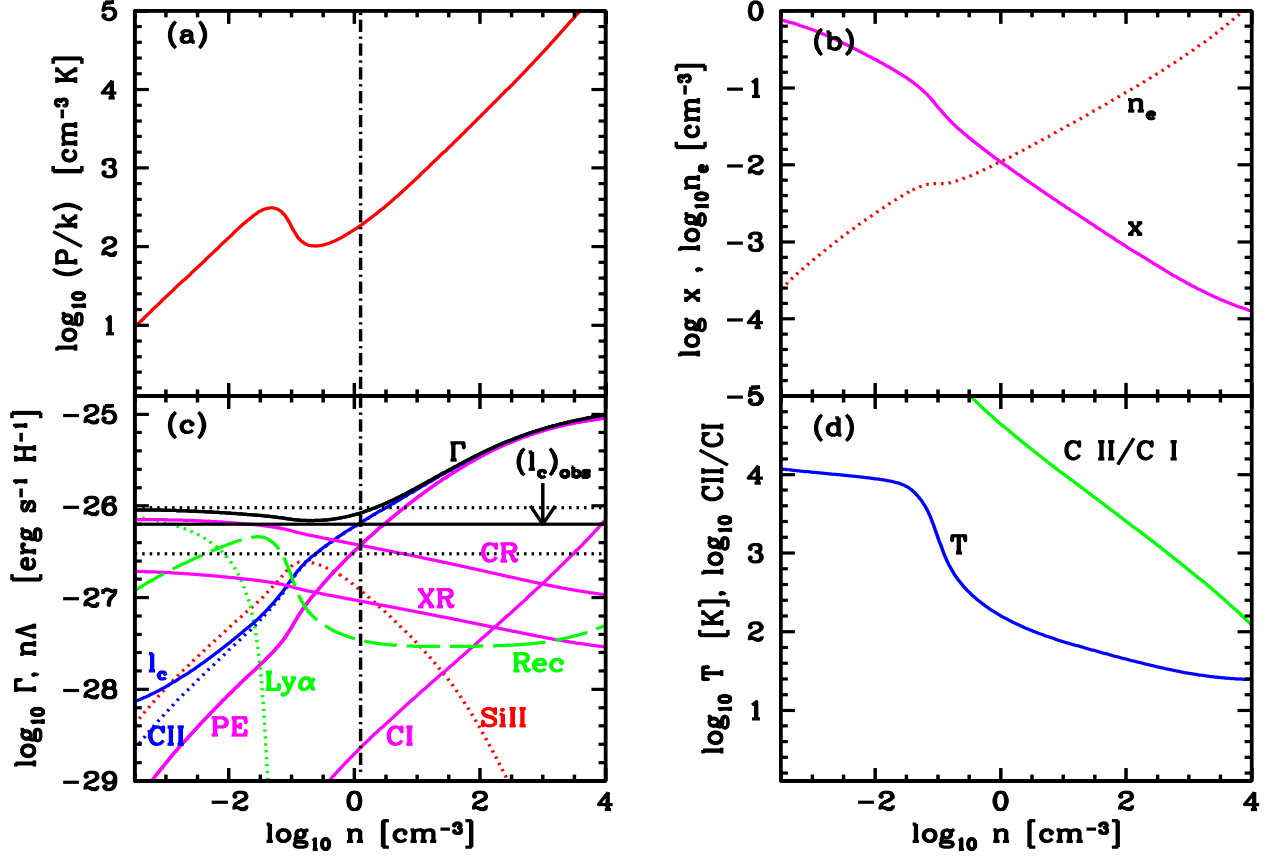


FIG. 6.— Two-phase diagrams for the $z = 1.919$ damped Ly α system toward Q2206–19. Same as Figure 2 except internal sources of heating are included. Specifically, grain photoelectric heating by starlight with FUV mean intensity, $J_{\nu}^{stars} = 1.7 \times 10^{-18}$ ergs cm⁻² s⁻¹ Hz⁻¹ sr⁻¹ is included. Heat inputs from locally generated soft X-rays and cosmic rays are also included (see text). This CNM solution yields agreement between $l_c(n)$ and l_c^{obs} at the CNM density, $n_{CNM} = 1.3$ cm⁻³. This is the thermally stable density in which CNM and WNM gas are in pressure equilibrium at pressure, $P = (P_{min} P_{max})^{1/2}$ (see text).

tion for the 95 % confidence lower and upper limits on l_c^{obs} . We then assumed the errors in J_{ν}^{stars} to be the differences between the limiting values of J_{ν}^{stars} and that corresponding to the mean l_c^{obs} . These errors are due to systematic uncertainties in l_c^{obs} , and are larger than the random statistical errors for this damped Ly α system. Other systematic errors arise from the uncertainty in P_{eq} , κ , and J_{ν}^{bkd} . To evaluate these we recomputed J_{ν}^{stars} by (1) letting P_{eq} vary between P_{min} and P_{max} , (2) varying κ between the conditions of minimal and maximal depletion, and (3) varying J_{ν}^{bkd} between 0.1 and 3.0 times the Haardt-Madau backgrounds used here, which are overestimates of the uncertainties in J_{ν}^{bkd} (Haardt & Madau 2003). Again assuming the variances are determined by the differences between these limiting values and the mean J_{ν}^{stars} defined by $P_{eq} = (P_{min} P_{max})^{1/2}$, we find that $J_{\nu}^{stars} = (1.7^{+2.7}_{-1.0}) \times 10^{-18}$ ergs cm⁻² s⁻¹ Hz⁻¹ sr⁻¹ for the CNM solution and $J_{\nu}^{stars} = (3.9^{+5.9}_{-2.3}) \times 10^{-17}$ ergs cm⁻² s⁻¹ Hz⁻¹ sr⁻¹ for the WNM solution. The latter two are the means of the minimal and maximal depletion “WD-low” solutions and the errors correspond to 95 % confidence intervals. In every case the J_{ν}^{stars} predicted by the WNM solutions exceed the 95 % confidence upper limit

for our CNM solution. These estimates for the “WD-low” model are also consistent with the predictions of most “WD-high” and “BT” solutions. Figure 7 plots the CNM solutions of J_{ν}^{stars} versus $J_{\nu}^{bkd} / (J_{\nu}^{bkd})_{HM}$, where $(J_{\nu}^{bkd})_{HM}$ is the Haardt-Madau background solution adopted here. We computed solutions for all the three grain models used in this paper. Comparison with the above estimate of J_{ν}^{stars} for the CNM model shows consistency between the “WD-high”, “BT”, and “WD-low” models with the possible exception of the “BT” model, which predicts J_{ν}^{stars} to be slightly lower than our estimate.⁷

Finally, it is interesting that these are the highest in-

⁷Note, J_{ν}^{stars} predicted by the “WD-high” model is larger than predicted by the “WD-low” model. This seemingly contradicts the higher heating efficiency of the “WD-high” model, because J_{ν}^{stars} required to produce a given heating rate decreases with increasing heating efficiency. However, that argument holds for a given density. Because of the high metallicity of the Q2206A damped Ly α system and the shape of the heating function, $\Gamma_d(n)$, the value of n_{CNM} is lower for the “WD-high” than for the “WD-low” model. As the density decreases, J_{ν}^{stars} increases in order to balance the cooling rate, l_c^{obs} . This effect is more important in the Q2206A damped Ly α system than the heating heating efficiency effect, which is why J_{ν}^{stars} is higher for the “WD-high” model. Note, J_{ν}^{stars} for the “WD-high model” is smaller than for the “WD-low model” for every other damped Ly α system in our sample.

tensities derived with the C II* technique for any damped Ly α system in our sample. This may explain why Q2206A is the only confirmed damped Ly α system yet detected in emission at high redshift.

4.2. J_ν Inferred from Direct Detection of Starlight

Møller et al. (2002) obtained a STIS image of the Q2206–19 field with a very wide V filter in which the effective central wavelength is 5851.5 Å and FWHM=4410.3 Å. The image has an angular resolution of 0.08 arcsec. The field shows a diffuse galaxy with an irregular shape and a bright knot from which Ly α emission is detected. The identification of the galaxy with the damped Ly α system follows from the redshift of Ly α emission, which is 250 ± 50 km s $^{-1}$ larger than the absorption-line redshift. With an angular separation of $\theta_b=0.99$ arcsec, the impact parameter of the knot with respect to the QSO sightline is given by $b=8.4$ kpc for the WMAP (Bennett et al. 2003) cosmological parameters adopted here. From their STIS photometry of the galaxy, Møller et al. (2002) found $V = 24.69 \pm 0.07$ within a circular aperture radius of 0.3 arcsec, where V is the “ V ” magnitude corresponding to a filter with central wavelength $\lambda = 5851.5$ Å. More recently, [O III] 5007 emission with a redshift similar to that of Ly α emission was detected from the object labeled “ps”, which is located within ≈ 0.8 arcsec of the bright knot (Warren 2004).

To test the predictions of the C II* model we determine J_ν at the the location of the absorbing gas. Summing over pixels coinciding with the associated galaxy in the STIS image, we find

$$J_\nu = \frac{(1+z)^3}{4\pi} \sum_i \frac{F_{\nu_0}^i}{\theta_i^2}, \quad (6)$$

where we assume the physical distance between each pixel and the absorbing gas equals its projection on the sky. Here $F_{\nu_0}^i$ is the flux density in the i^{th} pixel, which is separated from the brightness centroid of the QSO by the angle θ_i and detected at frequency $\nu_0 = \nu(1+z)^{-1}$, where the rest wavelength corresponding to ν is $\lambda = 2000$ Å. In the presence of dust, the sum in equation (6) would contain the extinction correction, $\exp[\tau_{\parallel}^i - \tau_{\perp}^i]$, where τ_{\parallel}^i and τ_{\perp}^i are the 2000 Å dust optical depths along the line of sight to pixel i and between pixel i and the absorbing gas in the plane of the galaxy. Independent estimates of τ_{\parallel}^i indicate that it varies with θ_i . The depletion pattern implied by the ratio $[\text{Fe}/\text{Si}]_{\text{gas}}$ suggests $\tau_{\parallel}^i \approx 0.05$ to 0.10 along the QSO sightline. To estimate τ_{\parallel}^i at the Ly α -emitting bright knot, we refer to observations of Lyman Break Galaxies (LBGs). Shapley et al. (2003) show that E_{B-V} for LBGs to decrease with increasing Ly α equivalent width, W . Since $W = 88$ Å, we infer $E_{B-V} \approx 0.06$, and as a result $\tau_{\parallel}^i \approx 0.5$ at the position of the knot. However, owing to the irregular light distribution, the main contribution to the sum comes from pixels closer to the QSO sightline than the knot; i.e., from locations where $\tau_{\parallel}^i \ll 0.5$. Since $\tau_{\perp}^i \ll 0.5$ in the limit $\theta^i \rightarrow 0$, the dust correction to equation (6) can be safely ignored.

The expression for J_ν in eq. (6) was kindly evaluated for us by P. Møller (2004), who summed $F_{\nu_0}^i/\theta_i^2$ from an

inner radius surrounding the QSO, θ_{min} , to an outer radius, θ_{max} . We found the result to be insensitive to the choice of θ_{max} for $\theta_{\text{max}} \geq 0.75$ arcsec, since irregularities in the outer brightness distribution such as the bright knot contributes less than 10 % to the total J_ν . For this reason we let $\theta_{\text{max}} = 1.5$ arcsec. But the results are sensitive to the value of θ_{min} as it approaches the radius of the QSO PSF. We are confident the result is not dominated by PSF subtractions errors when $\theta_{\text{min}}=0.36$ arcsec. In this case we obtain a lower limit of $J_\nu^{\text{phot}}=3.8 \times 10^{-18}$ ergs cm $^{-2}$ s $^{-1}$ Hz $^{-1}$ sr $^{-1}$, where we have introduced the quantity J_ν^{phot} to avoid confusion with the C II* technique. On the other hand when $\theta_{\text{min}} \leq 0.21$ arcsec, the result is completely dominated by PSF subtraction errors. Therefore, we obtain the “upper limit” $J_\nu^{\text{phot}}=7.0 \times 10^{-18}$ ergs cm $^{-2}$ s $^{-1}$ Hz $^{-1}$ sr $^{-1}$ when $\theta_{\text{min}} = 0.21$ arcsec. The latter result is not a true upper limit because point sources hidden within the PSF could raise J_ν^{phot} significantly. For example, if the bright knot were located within 0.1 arcsec of the QSO sightline, its contribution to J_ν^{phot} would be a factor of 10 larger than that of the entire galaxy. We shall ignore this improbable configuration and assume a uniform light distribution at $\theta < \theta_{\text{min}}$. From our solution to the transfer equation in WPG (see their eqs. (14) and (18)) we find comparable contributions to J_ν^{phot} from sources on either side of the $\theta = \theta_{\text{min}}$ boundary. For this reason we conclude that $J_\nu^{\text{phot}}=(3.8 \rightarrow 14.0) \times 10^{-18}$ ergs cm $^{-2}$ s $^{-1}$ Hz $^{-1}$ sr $^{-1}$.

4.3. Comparison Between C II* and Photometric Estimates of J_ν

Let us compare the photometric estimate of J_ν with the predictions of the C II* technique. From § 4.1 we have $J_\nu^{\text{CII}^*}=(1.7_{-1.0}^{+2.7}) \times 10^{-18}$ ergs cm $^{-2}$ s $^{-1}$ Hz $^{-1}$ sr $^{-1}$ for the CNM model, and $J_\nu^{\text{CII}^*}=(38_{-23}^{+52}) \times 10^{-18}$ ergs cm $^{-2}$ s $^{-1}$ Hz $^{-1}$ sr $^{-1}$ for the WNM model, where in the present subsection we have substituted the quantity $J_\nu^{\text{CII}^*}$ for J_ν^{stars} to avoid confusion with the photometric results (see Table 3). Since these intensities are evaluated at $\lambda=1500$ Å, and J_ν^{phot} obtained from the photometric technique corresponds to $\lambda=2000$ Å, the spectral shape of the FUV continuum could be a source of additional errors. But such errors are negligible since the continuum is observed to be flat (Møller et al. 2002), and theoretical models of star forming regions predict the continuum to be flat (Bruzual & Charlot 2003). These estimates of $J_\nu^{\text{CII}^*}$ are compared with the estimates of J_ν^{phot} in Table 3. Because the latter estimates were made by equating the projected and physical separations between the galaxy and the absorbing gas, the results for J_ν^{phot} are upper limits. As a result, the limits on J_ν^{phot} are consistent with the values of $J_\nu^{\text{CII}^*}$ predicted for the CNM, but not the WNM model. The discrepancies with the WNM model are larger than may be apparent because the error bars on $J_\nu^{\text{CII}^*}$ correspond to 2- σ upper and lower limits set by estimates of the C II* column density rather than 1- σ random errors obtained from the uncertainties in $N(\text{H I})$ and to a lesser extent, $N(\text{C II}^*)$.

The results in Table 3 are also illustrated in Figure 7, which compares the photometric upper limit on J_ν^{phot} (horizontal line) corresponding to $\theta_{\text{min}} = 0.21$ arcsec with

TABLE 3

MEAN INTENSITIES FROM PHOTOMETRIC AND C II*
TECHNIQUES

Technique	Approximation	J_ν^{stars} ^d	Notation
Photometry	θ_{min} ^a =0.36 arcsec	<3.8 ^b	J_ν^{phot}
Photometry	θ_{min} ^a =0.21 arcsec	<14.0 ^b	J_ν^{phot}
C II*	CNM	$1.7^{+2.7}_{-1.0}$ ^c	$J_\nu^{CII^*}$
C II*	WNM	38^{+52}_{-23} ^c	$J_\nu^{CII^*}$

^aInner radius used to obtain J_ν from eq. (6). Outer radius, θ_{max} =1.5 arcsec.

^b95 % confidence upper limit obtained by equating physical and projected separations between galaxy pixels and the QSO sightline

^c95 % confidence errors

^d 10^{-18} [ergs cm⁻² s⁻¹ Hz⁻¹ sr⁻¹]

$J_\nu^{CII^*}$ predicted by the CNM model (empty triangle with vertical error bars). The true value of J_ν^{phot} , $(J_\nu^{phot})_{true}$, depends on the inclination angle, i , of the galaxy to the line of sight such that $(J_\nu^{phot})_{true} = \cos^2(i) J_\nu^{phot}$. From Figure 7 we see that compatibility between $(J_\nu^{phot})_{true}$ and $J_\nu^{CII^*}$ is obtained for $0^\circ < i < 77^\circ$; i.e., for a wide range of plausible inclination angles. In the case of the ‘BT’ model and $J_\nu^{bkd} \geq 1.7(J_\nu^{bkd})_{HM}$, an inclination angle, exceeding 85° is required, which has a probability less than 0.7 %. Nevertheless, the uncertainties are sufficiently small for us to draw an important conclusion: we find a self-consistent model in which [C II] 158 μ m cooling is balanced by the heating rate supplied by the FUV radiation field of the galaxy associated with this damped Ly α system, provided C II* absorption arises in CNM gas.

5. ARE ALL DAMPED Ly α SYSTEMS INTERNALLY HEATED BY RADIATION ?

If the Q2206A damped Ly α system is heated by local starlight, it is plausible to ask whether all damped Ly α systems are heated in the same manner. This is a natural question to pose for the damped Ly α systems with positive detections of C II* absorption since internal heat sources are required in most cases (see § 3.2). Indeed WPG assumed the presence of internal radiation fields to deduce J_ν^{stars} for their sample of 33 damped Ly α systems. While they ignored the background contribution to J_ν , the $l_c(n)$ curves in Figure 3 show that background heating can be appreciable, especially for the ‘WD-high’ and ‘BT’ models. Therefore in § 5.1 we recompute J_ν^{stars} in the presence of background radiation for damped Ly α systems with positive detections. We shall also examine the role of local radiation for damped Ly α systems with upper limits on C II* absorption. In § 3.2 we showed that background heating alone could account for [C II] 158 μ m emission from these objects if the true value of l_c^{obs} were sufficiently low. In § 5.2 we shall determine whether the upper limits are also consistent with the presence of local radiation fields.

5.1. Systems with Positive Detections

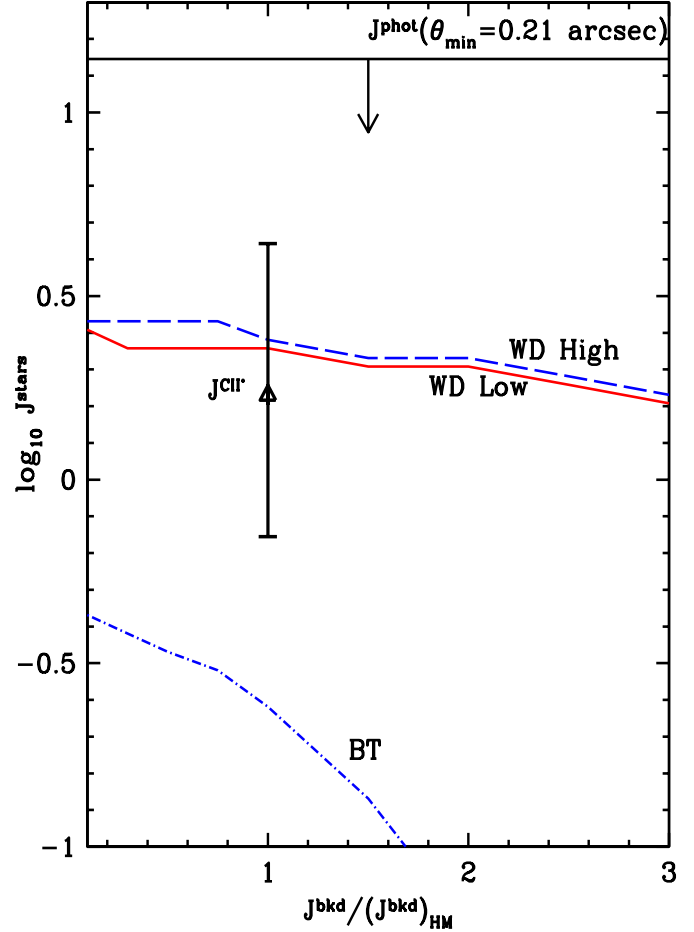


FIG. 7.— J_ν^{stars} solutions for Q2206A damped Ly α system versus $J_\nu^{bkd}/(J_\nu^{bkd})_{HM}$ where $(J_\nu^{bkd})_{HM}$ is Haardt-Madau (2003) background radiation field used throughout this paper and J_ν^{stars} is in units of 10^{-18} ergs cm⁻² s⁻¹ Hz⁻¹ sr⁻¹. Curves are dot-dashed for the ‘BT’ model, dashed for the ‘WD-high’ model, and solid for the ‘WD-low’ model. Unfilled triangle labeled ‘ J^{CII^*} ’ is our estimate of J_ν^{stars} for ‘WD-low’ model, where the data point is an average of the maximal and minimal depletion models. Error bars include systematic errors due to uncertainties in κ , P_{eq} , and J_ν^{bkd} (see text). The ‘WD-low’ solid curve was computed for minimal depletion. Horizontal line denoted by $J^{phot}(\theta_{min}=0.21$ arcsec) is upper limit on J_ν^{phot} inferred from photometry of associated galaxy when $\theta_{min}=0.21$ arcsec (see text).

We obtained J_ν^{stars} for 23 damped Ly α systems with positive detections of C II* absorption (see Table 2). In each case we followed the same procedures used in § 4.1, in particular we added J_ν^{bkd} and J_ν^{stars} to compute the total mean intensity, J_ν , illuminating the gas, and then considered only solutions in which C II* absorption arises in CNM gas at the thermally stable density, n_{CNM} . Currently detected C II* absorption is unlikely to arise in WNM gas for most damped Ly α systems with positive detections (see § 4). In the case of the ‘WD-low’ CNM model the J_ν^{stars} derived with the addition of background radiation was typically 0.1 dex less than the J_ν^{stars} derived without background radiation. On the other hand, our calculations admitted no CNM solutions for J_ν^{stars} in the damped

Ly α systems toward Q2241+13 and Q1036–22: this is not surprising in view of the significant contribution of the high redshift CMB radiation to the $l_c(n)$ solutions shown in Figure 3b. The largest discrepancies for damped Ly α systems that admitted CNM solutions were Q1346–03 and Q0255+00 for which J_ν^{stars} with background radiation was 0.55 dex and 0.15 dex less than without background radiation. However, these four damped Ly α systems more closely resemble most systems with upper limits because l_c^{obs} is less than or equal to the peak of the predicted $l_c(n)$ curve. In § 5.2 we show that in systems like this, the line of sight likely passes through WNM gas subjected to a range of J_ν^{stars} including those inferred for the CNM solutions.

Because of the low fraction of discrepant estimates of J_ν^{stars} and since the discrepancies are confined to objects with the lowest values determined for J_ν^{stars} , we conclude that background radiation has little effect on the SFRs derived by WPG for the “WD-low” model. Specifically, the average J_ν^{stars} decreased by only 0.04 dex when background radiation was included in the models. This quantity has cosmological significance since the average J_ν^{stars} can be used to deduce the average SFR per unit area from which one can deduce the global SFR per unit comoving volume (see WGP). The same qualitative arguments hold for the “WD-high” and “BT” models. The average J_ν^{stars} decreased by 0.15 dex when background radiation was included in the “BT” model and by 0.3 dex for the “WD-high” model.

5.2. Systems With Upper Limits

The nature of damped Ly α systems with upper limits on C II* absorption is determined by the ratio of the true value of l_c^{obs} to the peak value of $l_c(n)$ predicted for background heating alone, l_c^{peak} . This point is illustrated in Figure 8, which shows $l_c(n)$ curves predicted by the “WD-low” model for the Q2348–14 and Q2237–06 damped Ly α systems. These objects were selected to represent the highest and lowest values of the ratio l_c^{obs}/l_c^{peak} in Figure 4. We computed $l_c(n)$ curves for the case $J_\nu = J_\nu^{bkd}$. This results in the lowest $l_c(n)$ curves in Figure 8 (shown as red dotted curves), which correspond to background heating alone. We then let $J_\nu = J_\nu^{bkd} + J_\nu^{stars}$ to account for the presence of local radiation and computed $l_c(n)$ for the same grid of SFRs per unit area, $-4.0 < \log_{10}\psi_* < 0.0$ M $_\odot$ yr $^{-1}$ kpc $^{-2}$, used to find J_ν^{stars} for the Q2206A damped Ly α system. This corresponds to mean intensities in the range $5 \times 10^{-21} < J_\nu^{stars} < 5 \times 10^{-17}$ ergs cm $^{-2}$ s $^{-1}$ Hz $^{-1}$ sr $^{-1}$ at $\lambda = 1500$ Å (see WPG and § 5.1). By comparison, $J_\nu^{bkd} = 2.7 \times 10^{-20}$ and 2.0×10^{-20} ergs cm $^{-2}$ s $^{-1}$ Hz $^{-1}$ sr $^{-1}$ at the redshifts of the Q2348–14 and Q2237–06 damped Ly α systems. The $l_c(n)$ solutions including J_ν^{stars} are shown as solid curves in the Figure 8.

First, we consider the results shown in Figure 8a for Q2348–14. In this case the upper limit on l_c^{obs} ($10^{-26.9}$ ergs s $^{-1}$ H $^{-1}$) is significantly higher than l_c^{peak} ($10^{-27.4}$ ergs s $^{-1}$ H $^{-1}$). If future spectroscopy shows the true value of l_c^{obs} to remain above l_c^{peak} , then l_c^{obs} could intersect WNM or CNM thermally stable solutions corresponding to a wide range of J_ν^{stars} : the (n, l_c) coordinates of these stable solutions are respectively shown as the steeply rising dot-dashed and solid curves in Figure 8a. The crosses in Figure 8a depict upper limits on n set by the

C II/C I constraints for each $l_c(n)$ curve. Because these density limits are less than n_{CNM} , they appear to rule out the CNM solutions. However, WGP showed the limits to be sensitive to local input parameters such as X-ray and cosmic-ray ionization rates. For these reasons we make the conservative estimate that the CNM models are not excluded for upper limits on n exceeding $\approx 0.2n_{CNM}$. Therefore, if $l_c^{obs} > l_c^{peak}$, the CNM and WNM models are in principle equally plausible for this damped Ly α system. But, because we have found direct evidence against the WNM hypothesis for other damped Ly α systems with similar ratios of l_c^{obs} to l_c^{peak} (see Howk et al. 2004 a,b) we believe the CNM hypothesis to be more likely in these cases.

On the other hand, the CNM solutions for Q2348–14 are implausible if $l_c^{obs} < l_c^{peak}$. The presence of background radiation causes a significant increase in $l_c(n)$ for low values of J_ν^{stars} . The result shown in Figure 8a is that no thermally stable CNM solutions are possible for l_c^{obs} less than the intersection of the background heated $l_c(n)$ and the locus of thermally stable CNM solutions; i.e., when $l_c^{obs} < 10^{-27.5}$ ergs s $^{-1}$ H $^{-1}$. By contrast, the WNM solutions, thermally stable or otherwise, are consistent with the condition $l_c^{obs} < l_c^{peak}$ for the entire grid of J_ν^{stars} .

The low densities, $n < 1$ cm $^{-3}$, predicted for models with large values of J_ν^{stars} argue in favor of moderate values of J_ν^{stars} ($< 10^{-18}$ ergs cm $^{-2}$ s $^{-1}$ Hz $^{-1}$ sr $^{-1}$). Otherwise the linear dimensions of the absorbing gas clouds would become implausibly large. It is important to note that X-ray heating dominates grain photoelectric heating in all the WNM solutions, and that the X-ray background dominates local X-ray sources for $J_\nu^{stars} < 5 \times 10^{-19}$ ergs cm $^{-2}$ s $^{-1}$ Hz $^{-1}$ sr $^{-1}$.

To investigate the effect of background radiation on these conclusions, we recomputed the $l_c(n)$ curves with the same procedures, but excluded all radiation backgrounds. The results are shown in Figure 8b. Without background heating no lower bound on thermally stable CNM solutions exists; i.e., the thermally stable CNM locus can extend to arbitrarily low values of $l_c(n)$. Therefore, when the effects of background radiation are omitted, CNM solutions with $l_c^{obs} < l_c^{peak}$ can exist in principle. But when background radiation is present and $l_c^{obs} < l_c^{peak}$, the C II/C I constraint results in upper limits on $n < 0.03n_{CNM}$ (Figure 8a). Because this discrepancy is larger than allowed by model uncertainties, we conclude that thermally stable CNM solutions are ruled out when $l_c^{obs} < l_c^{peak}$.

Next we consider the results for Q2237–06 in Figure 8c. In this case the existing upper limit on l_c^{obs} is less than l_c^{peak} and as a result all of the CNM solutions are ruled out. Because of the large redshift, $z=4.080$, the CMB dominates the behavior of $l_c(n)$ for low values of J_ν^{stars} . This is illustrated in Figure 8d, which plots the $l_c(n)$ curves that result in the absence of background radiation. Comparison with Figure 8c reveals two features caused by background radiation: a low-density asymptote at $l_c(n)=10^{-27.6}$ ergs s $^{-1}$ H $^{-1}$ due to CMB radiation, and an increased peak value, $l_c^{peak}=10^{-27.3}$ ergs s $^{-1}$ H $^{-1}$, due to the combination of CMB and X-ray background radiation. Again, Figure 8d shows that without background radiation, thermally stable CNM solutions would be possible. Note, the absence of density limits is due to the lack of a C II/C I constraint

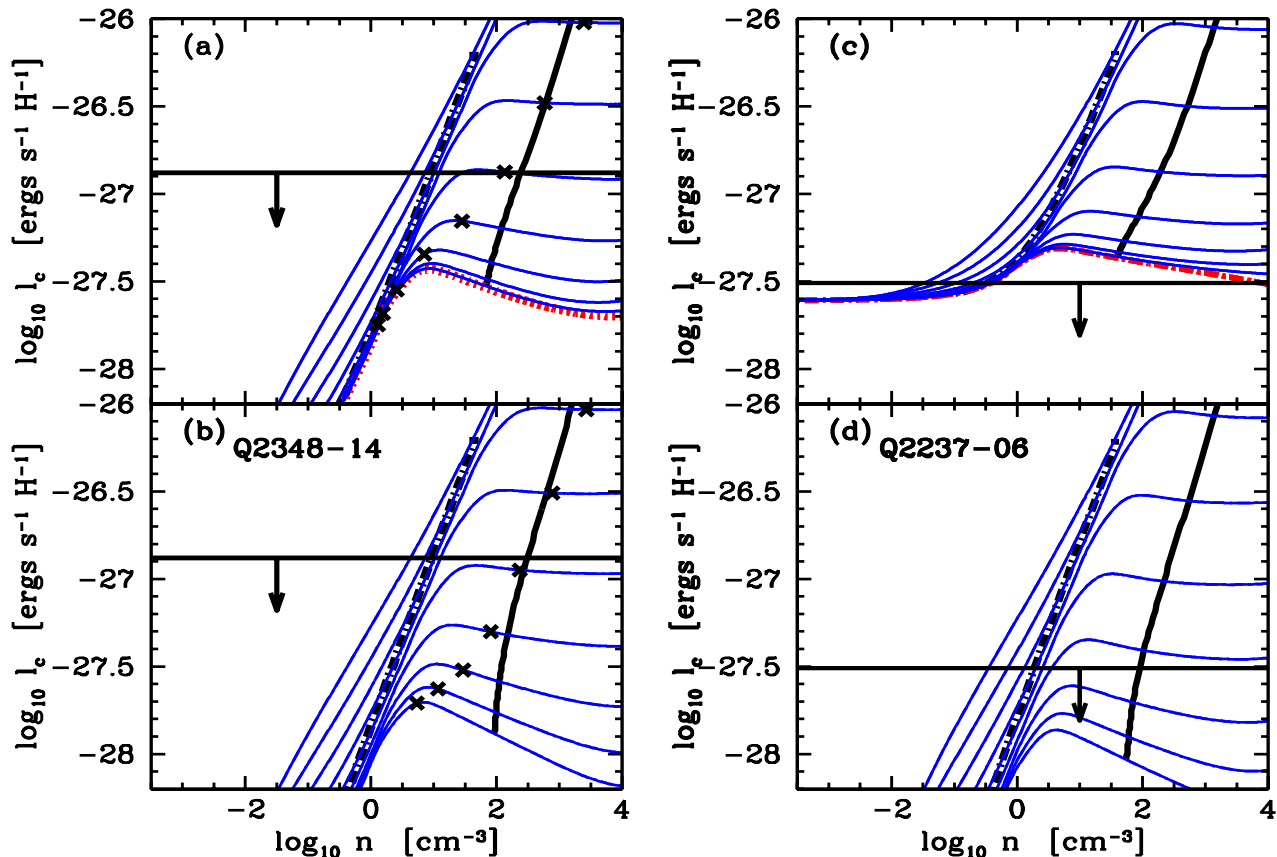


FIG. 8.— Solid curves are equilibrium $l_c(n)$ solutions for gas subjected to internal heating rates generated by a grid of SFRs per unit area, $\log_{10}\dot{\psi}_* = -4.0, -3.5, \dots, 0.0 M_\odot \text{ yr}^{-1} \text{ kpc}^{-2}$. Same form of FUV, X-ray, and cosmic-ray inputs as in Figure 6. (a) and (b) show results for the Q2348–14 damped Ly α system in which background radiation is included in (a) and excluded in (b). Lowest dotted curve in (a) is the result for background radiation alone. The horizontal line with arrow corresponds to $2\text{-}\sigma$ upper limit on l_c^{obs} . The steeply rising dot-dashed and solid curves are thermally stable WNM and CNM solutions at $n = n_{\text{WNM}}$ and n_{CNM} . Crosses are upper limits on n set by C II*/C I constraint for each $\dot{\psi}_*$. (c) and (d) are analogous results for Q2237–06 damped Ly α system. (see § 4.2 for discussion)

for this damped Ly α system.

Therefore, since $l_c^{\text{obs}}/l_c^{\text{peak}} < 10^{0.2}$ for most cases in Figures 4a and 4b, we predict the sightlines through most damped Ly α systems with upper limits on C II* absorption to pass through WNM gas alone. The same conclusion holds for the damped Ly α systems with positive detections for which $l_c^{\text{obs}}/l_c^{\text{peak}}$ are also less than $10^{0.2}$ (i.e., the damped Ly α systems toward Q0127–00, Q0255+00, Q1036–22, Q1346–03, and Q2241+13). In the few cases of upper limits with higher ratios of l_c^{obs} to l_c^{peak} , the sightlines could encounter either WNM or CNM gas. But the similar $l_c^{\text{obs}}/l_c^{\text{peak}}$ ratios for damped Ly α systems with positive detections, objects for which there is independent evidence favoring the CNM hypothesis (cf. WGP and Howk et al. 2004), suggests that in these cases the gas is CNM.

6. THE IMPACT OF IONIZED GAS ON THE C II* ANALYSIS

The thermal equilibria presented above were computed by assuming C II* absorption arises in neutral gas. But, C II* absorption could also arise in ionized gas. Since a significant fraction of the C II* absorption detected in the halo and thick gaseous disk of the Galaxy arises in a warm ionized medium (WIM; see Lehner, Wakker, & Savage 2004), the same may be true in damped Ly α systems.

Indeed, the presence of Al III, C IV, and Si IV absorption in most damped Ly α systems indicates that the QSO sightlines typically pass through ionized as well as neutral gas (Wolfe & Prochaska 2000a,b).

However, there are several reasons why C II* absorption in damped Ly α systems is unlikely to arise in ionized gas. First, from the constraint on the optical depth ratio, $\tau(\text{Si II}^* 1264.7)/\tau(\text{C II}^* 1335.7) < 10^{-2.5}$, Howk, Wolfe, & Prochaska (2004a) deduced an upper limit of $T < 800$ K for the $z=4.22$ damped Ly α system toward PSS 1443+27. C II* absorption cannot arise in ionized gas in this damped Ly α system because such gas typically has temperatures exceeding 10^4 K. Because there are indications of similar limits in at least two other damped Ly α systems, this temperature limit may be a generic property, which would rule out ionized gas as the site of C II* absorption in most damped Ly α systems. Second, consider the highly ionized gas, which gives rise to C IV and Si IV absorption. In a systematic study of 32 damped Ly α systems, Wolfe & Prochaska (2000a,b) found statistically significant differences between the velocity structure of the low ions and the high ions. Because the C II* velocity profiles are, with rare exceptions, indistinguishable from the low-ion resonance line profiles (WPG), C II* absorption is unlikely to

originate in highly ionized gas. This has interesting implications. The presence of narrow C IV absorption components with FWHM $< 30 \text{ km s}^{-1}$ implies $T < 2 \times 10^5 \text{ K}$, which indicates CIV is photoionized in damped Ly α systems. To summarize, although hot gas may be present, comparison between the velocity structure of the C IV and C II* absorption profiles suggests the two ions do not co-exist in the same gas, and the narrow C IV line widths indicate C IV is not directly tracing hot gas nor its interaction with cool gas.

On the other hand, Lehner, Wakker, & Savage (2004) present convincing evidence that a significant fraction of C II* absorption lines in the ISM arises in the WIM. Since the WIM of the ISM of the Galaxy is also the site of Al III absorption (Savage & Edgar 1990), the implication is that the gas giving rise to Al III absorption is also the site of C II* absorption. Because Al III absorption is a generic feature in the spectra of damped Ly α systems, and because of the similarity between the centroids of the multiple velocity components in the Al III and low-ion profiles (Wolfe & Prochaska 2000a), the close resemblance between the C II* and low-ion profiles suggests that C II* absorption in damped Ly α systems also arises in a WIM. However, this is unlikely. First, in some instances the ratio of Al III to low-ion column densities varies strongly with velocity (Wolfe & Prochaska 2000), indicating that Al III may not be an accurate tracer of C II* absorption in damped Ly α systems. Second, even if Al III does trace the low ions, Al III need not trace WIM gas in damped Ly α systems, since there are other means of producing Al III than stellar photons. At high redshifts a primarily neutral gas can contain significantly higher column densities of Al III than at $z=0$; i.e., at high z the presence of Al III need not be a signature of a WIM. This is due to the predicted increase with z of the soft X-ray background intensity (Haardt & Madau 2003): at $z > 2$ the background intensity at 0.5 keV (shown in Figure 1) should be more than 30 times higher than at $z = 0$. As a result, more radiation is available for photoionizing Al II (IP=18.8 eV) to Al III (IP=28.4 eV) than at $z=0$. Prochaska et al. (2002) find empirical evidence for this in the $z=2.62$ damped Ly α system toward Q1759+75, where comparison between intermediate and low-ion velocity profiles shows significant Al III absorption at the position of the velocity component associated with neutral gas.

These points are illustrated in Figure 9, which shows the results of a CLOUDY (Ferland 2001) photoionization calculation in which we simulated the damped Ly α system toward Q2206A with a slab with $N(\text{H I}) = 10^{20.5} \text{ cm}^{-2}$, $n=0.1 \text{ cm}^{-3}$, and $[\text{Fe}/\text{H}]=-1$. The slab is subjected to the same Haardt-Madau backgrounds (2003) as shown in Figure 1. While local inputs were neglected, these will have negligible effect on the Al II/Al III ratio or the (CI+CII)/C ratio. The x axis is the ionization parameter, the blue curve shows the [Al III/Al II] ratio, the red curve shows the linear neutral gas fraction, $1-x$, and the orange curve shows $\log_{10}(\text{CII}/\text{C})$. Since we have not measured Al II 1670 (which is undoubtedly saturated) we assume [Al II/Fe II]=0 which is found for the few damped Ly α systems in which Al II 1670 is unsaturated. In that case the observed ratio, [Al II/Al III] = 0.58 dex. The dotted vertical lines show that value ± 0.1 dex. The cor-

responding neutral gas fraction, $1-x$, runs from 0.86 to 0.95. Therefore, one can accommodate a fairly large Al III column density in a mainly neutral gas, which produces significant amounts of C II. Furthermore, Figure 9 reveals a subtle but important point on the multi-phase nature of the damped Ly α system. If one assumes a single phase, then the gas is $\approx 10\%$ ionized and cannot be considered a cold neutral medium. This result contradicts our assessment of the C II* profile and we are driven to a two-phase solution (WNM+CNM) in order to accommodate the Al III and C II* measurements. Assuming comparable H I column densities for the WNM and CNM phases, we find a solution with $\log U \approx -4.5$ for the CNM and $\log U \approx -3$ for the WNM, which gives an average Al II/Al III ratio consistent with our observations. Adopting $J_{\nu\text{H}} \approx 10^{-21.5}$ for the ionizing background radiation, we find the implied density values are consistent with the model presented in Figure 6, e.g., $\log_{10} n_{\text{CNM}} \approx 0.2 \text{ cm}^{-3}$. Note that this relatively low density for the CNM is due to the high metallicity of the system. In summation, the presence of Al III does not require a WIM and in fact the observed Al II/Al III ratio is consistent with one's expectation based on the two-phase models derived from the C II* observations.

Further evidence against the ionized gas hypothesis for C II* absorption can be found in Figure 10, which plots l_c^{obs} versus $N(\text{H I})$ for the sample of damped Ly α systems in Table 2. The data show no evidence for correlations between l_c^{obs} and $N(\text{H I})$: the Kendall tau test reveals the probability for the null hypothesis of no correlations to be 65 %. By contrast, in a recent study of C II* absorption in the ISM, Lehner, Wakker, & Savage (2004) find a systematic increase in l_c^{obs} with decreasing $N(\text{H I})$, which they reasonably attribute to an increase in ionization level in systems with low $N(\text{H I})$. To understand this we note that in the absence of radiative excitation, $l_c^{\text{obs}} = n \Lambda_{\text{CII}} (1-x)^{-1}$, where $n \Lambda_{\text{CII}}$ is the 158 μm cooling rate per particle. In the low-density, high-ionization limit applicable here, $l_c^{\text{obs}} \propto J_{\nu\text{H}}$, where $J_{\nu\text{H}}$ is the radiation mean intensity at the Lyman limit. As a result, l_c^{obs} will increase with increasing $J_{\nu\text{H}}$, which causes $N(\text{H I})$ to decrease for a fixed total column density. By contrast, we find no convincing evidence for such an anti-correlation at $N(\text{H I}) \geq 2 \times 10^{20} \text{ cm}^{-2}$, which is additional evidence supporting the hypothesis that C II* absorption in damped Ly α systems arises in mostly neutral gas.

Finally, our arguments against background radiation as the heat source source for damped Ly α systems with positive detections of l_c^{obs} depended on the upper limits on the total density, n , inferred from photoionization equilibrium between C II and C I. The C II/C I ratios and the resultant density limits were computed for gas that was mainly neutral, and in the WNM phase for most cases. While ionized gas may not be the site of C II* absorption, it may still be present and could contribute to the total $N(\text{C II})$. Taking the results discussed above for Q2206A, in which $x < 0.14$, and assuming $N(\text{C I})=0$ and $N(\text{C II})=(\text{C}/\text{H})N(\text{H})_{\text{WIM}}$ for the WIM (where $N(\text{H})$ is the total column density of H), then the total C II column density, $N(\text{C II})=(\text{C}/\text{H})(N(\text{H})_{\text{WIM}}+N(\text{H})_{\text{WNM}}) \approx (1/0.86) \times (\text{C}/\text{H})N(\text{H I}) = 1.16(\text{C}/\text{H})N(\text{H I})$. Since the results are the same for $N(\text{C I})$, the change in the C II/C I ratio will

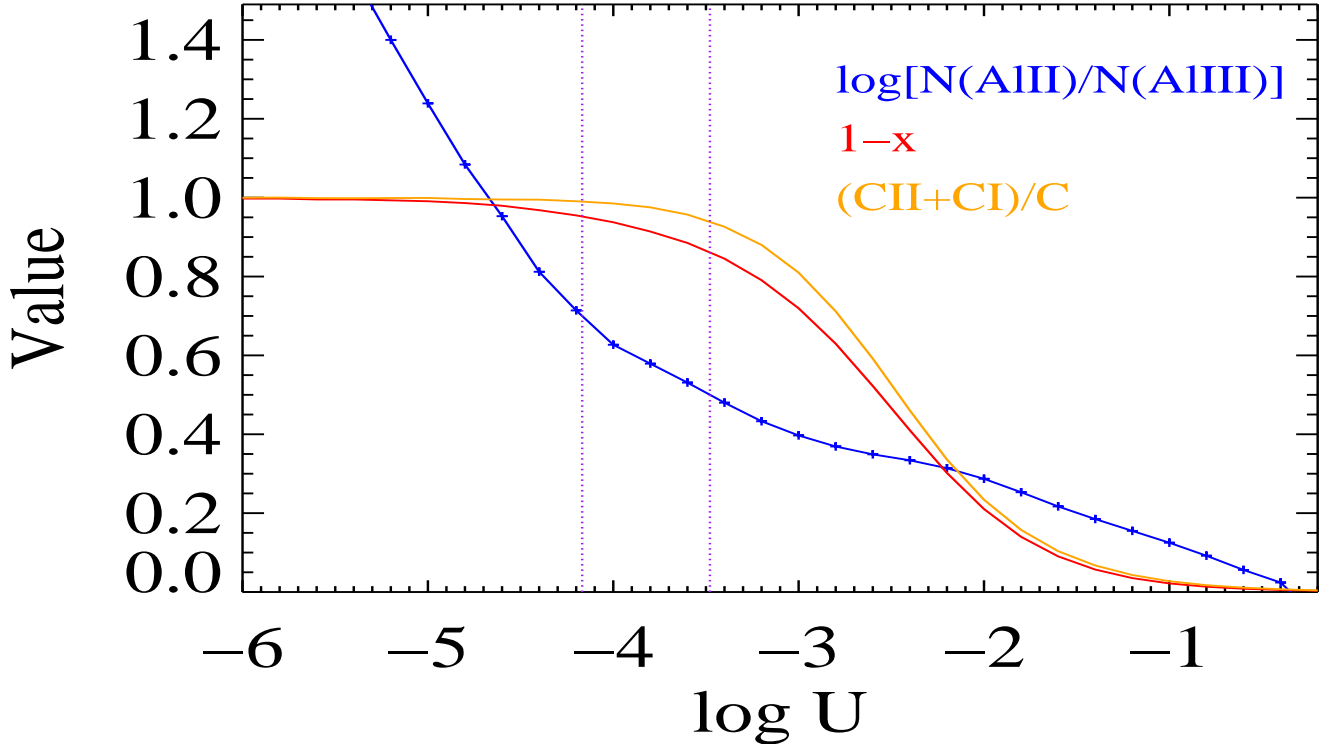


FIG. 9.— Various ionization ratios versus ionization parameter resulting from simulation of photoionization equilibrium for the Q2206A damped Ly α system. We let ionizing background radiation be incident on a plane parallel slab with $N(\text{H I}) = 10^{20.5} \text{ cm}^{-2}$, $n = 0.1 \text{ cm}^{-3}$, and $[\text{Fe}/\text{H}] = -1$. Blue curve is $[\text{AlII}/\text{AlIII}]$, red curve is linear neutral gas fraction, $1-x$, and orange curve is $(\text{CII}+\text{CI})/\text{C}$.

be at most 16%. This is insufficient to alter the conclusions given in § 3.1.

To summarize, by contrast with the ISM, the evidence accumulated so far suggests that the WIM does not give rise to significant C II* absorption in damped Ly α systems. While an investigation of the difference in physical conditions is beyond the scope of this paper, we suggest two possibilities: (1) an extensive WIM may not be present in damped Ly α systems owing to a low escape fraction of ionizing radiation from H II regions embedded in the neutral gas. This is consistent with the presence of Al III, the main indicator of the WIM in the ISM, since Al III can arise in neutral gas in damped Ly α systems due to the increased strength of the X-ray background at large redshifts. (2) If an extensive WIM does exist in damped Ly α systems, C II* absorption is suppressed because of the low value of (C/H) and possibly because the mean electron density is lower than in the neutral ISM (see eq. 4). Lower electron densities could result from gas pressures, which are lower than in the CNM/WNM interface.

7. CONCLUDING REMARKS

Our main conclusions are:

(1) Most damped Ly α systems with positive detections of C II* λ 1335.7 absorption are not heated by external background radiation, but rather require an internal energy source.

(2) The internal energy source for one such object, the Q2206A damped Ly α system, appears to be FUV radiation emitted by stars in the associated galaxy identified by Møller et al. (2002). In this case, C II* absorption cannot

arise in WNM gas, but rather arises in CNM gas.

(3) Independent arguments, in particular the strong correlation between l_c^{obs} and dust-to-gas ratio, suggest C II* absorption currently detected in most damped Ly α systems also arises in CNM gas that is similarly heated.

(4) Damped Ly α systems with upper limits on C II* absorption also require internal energy sources if the true values of l_c^{obs} exceed the peak values of $l_c(n)$ predicted for heating by background radiation alone, l_c^{peak} . While the absorbing gas could in principle be either CNM or WNM, the resemblance of the ratio l_c^{obs}/l_c^{peak} to most systems with positive detections suggests the gas is CNM.

(5) For most damped Ly α systems with upper limits the true values of l_c^{obs} are likely to be less than l_c^{peak} . In this case the gas could be heated by background radiation alone. But the data are also consistent with the added presence of internal energy sources. In either case, absorption is likely to arise in WNM gas. The same conclusion holds for the few damped Ly α systems with positive detections and in which l_c^{obs} is also less than l_c^{peak} .

(6) In the case of radiative heating, the radiation intensities deduced for the positive detections and allowed by the upper limits are about the same; i.e. $10^{-19} < J_\nu^{stars} < 10^{-18} \text{ ergs cm}^{-2} \text{ s}^{-1} \text{ Hz}^{-1} \text{ sr}^{-1}$. If the radiation is emitted from a uniform distribution of stars in a disk, the range of SFRs per unit area is given by $10^{-3} < \dot{\psi}_* < 10^{-2} \text{ M}_\odot \text{ yr}^{-1} \text{ kpc}^{-2}$ (see WPG). Therefore, all damped Ly α systems may be drawn from a single parent population of two-phase gas layers for which the strength of C II* absorption depends only on the phase encountered by the line of sight through the damped Ly α system. In the case

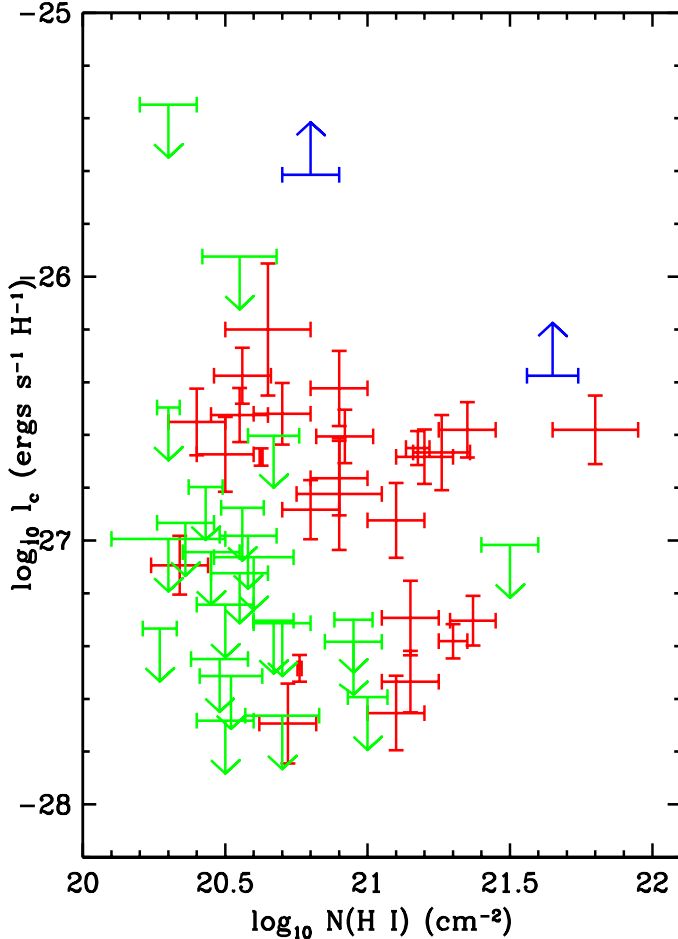


FIG. 10.— l_c^{obs} versus $N(\text{H I})$. Solid red, green, and blue data points are positive detections, 95 % confidence upper limits, and 95 % confidence lower limits for damped Ly α systems in Table 2.

of strong C II* absorption, the gas includes a CNM with $T \sim 100$ K and $n \sim 10 \text{ cm}^{-3}$, and for weak absorption the gas is WNM alone with $T \sim 8000$ K and $n \sim 10^{-1} \text{ cm}^{-3}$. Therefore, detectability of C II* absorption appears to depend only on the density of the gas encountered by the line of sight.

(7) By contrast with the ISM, the evidence accumulated so far suggests that C II* absorption in damped Ly α systems does not arise in a WIM.

The arguments against background radiation as the dominant source of heat input for damped Ly α systems with positive detections of C II* absorption are robust as they are insensitive to the properties of the dust responsible for grain photoelectric heating. Because of the low values of J_ν^{bkd} , the large lower limits on C II/C I imply small upper limits on n , typically $n < 0.03 \text{ cm}^{-3}$ (see equation 5). In that case the gas is restricted to the WNM phase where the predicted $158 \mu\text{m}$ emission rate, $l_c(n)$, is not tied to the grain photoelectric heating rate. Instead, $l_c(n)$ depends on n_e , which is well determined for the input quantities n and J_ν^{bkd} , and the fine-structure collision strength, which is accurately determined. We also find that $l_c(n)$ in the WNM is insensitive to variations in background intensity: when we increased J_ν^{bkd} by a factor of 10, $l_c(n)$ in the WNM in-

creased by only 0.2 dex. However, to relate temperature to density we assumed thermal equilibrium, which may not be applicable owing to the relatively long cooling times of the WNM (cf. Wolfire et al. 2003). But it is difficult to envisage any scenario in which $158 \mu\text{m}$ emission from gas at such low densities depends on grain properties.

By contrast, the conclusions concerning the heat source for the Q2206A damped Ly α system are sensitive to the nature of the dust responsible for grain photoelectric heating, because it is so metal rich. Specifically, J_ν^{stars} for the “BT” model is between factors of 3 to 5 lower than for the other models. The differences are related to differences in heating efficiencies, and differences in the predicted values of n_{CNM} . Despite this, the agreement between our estimates of J_ν^{phot} and J_ν^{stars} (illustrated in Figure 7) indicates that FUV starlight emitted by the galaxy associated with this DLA is incident on the grains associated with the gas and heats the gas by the grain photoelectric mechanism. This further argues against mechanical heating mechanisms such as turbulent dissipation (see discussion by Wolfire et al. 2003). We emphasize that the agreement holds only for the CNM model, since the WNM predictions for all three grain models indicates J_ν^{stars} exceeds the 95 % confidence upper limit on J_ν^{phot} . This result is in agreement with the conclusions reached by WPG and WGP who found that the bolometric background intensity predicted at $z = 0$ if the WNM model applies to all damped Ly α systems violated observational constraints. We also emphasize that the J_ν^{stars} predicted for this damped Ly α system are the highest in our sample, which may help to explain why Q2206A is the only confirmed damped Ly α system detected in emission at high redshift.

Finally, we consider the SFR of the Q2206A damped Ly α system. Summing over the same pixels used to determine J_ν^{stars} in equation (6), we can estimate the total FUV flux density of the associated galaxy. Assuming again that $\theta_{max} = 1.5$ arcsec, we find that $V=23.0$ if $\theta_{min}=0.36$ arcsec and $V=22.9$ if $\theta_{min} = 0.21$ arcsec; i.e., the results are insensitive to the value of θ_{min} . We also find they are insensitive to the value of θ_{max} for $\theta_{max} > 1.0$ arcsec. Assuming $V=23$ we find that the luminosity per unit bandwidth, $L_\nu=(2.0\pm 0.5)\times 10^{29} \text{ ergs s}^{-1} \text{ Hz}^{-1}$ where we have adopted conservative 25 % errors for the photometry. As a result $\text{SFR} = (26\pm 6.5)\text{M}_\odot \text{ yr}^{-1}$. Because we have not corrected for the effects of extinction, this is a lower limit. Following the discussion in § 4.2 in which we used the equivalent width of Ly α emission to estimate E_{B-V} we find that $\text{SFR} < 50 \text{ M}_\odot \text{ yr}^{-1}$. Comparison with LBGs, which are drawn from a Schechter luminosity function characterized by $(\text{SFR})_* = 60 \text{ M}_\odot \text{ yr}^{-1}$ and $\alpha = 1.6$ (Steidel et al. 1999; Shapley et al. 2003) shows the Q2206A galaxy to be an LBG with a typical SFR. On the other hand its irregular and extended morphology is atypical for LBGs and may be atypical for galaxies associated with damped Ly α systems. For this reason it is not obvious that these results can be extrapolated to other damped Ly α systems with detected C II* absorption by simply scaling SFR with J_ν^{stars} . Indeed, applying the simple uniform disk model of WPG and WGP to Q2206A, we find $\dot{\psi}_* = 0.03 \text{ M}_\odot \text{ yr}^{-1} \text{ kpc}^{-2}$ rather than the observed value of $\dot{\psi}_* > 1 \text{ M}_\odot \text{ yr}^{-1} \text{ kpc}^{-2}$. The latter value of $\dot{\psi}_*$ is consistent with the derived value of J_ν^{phot} because of

the small solid angle subtended by the FUV continuum sources from the location of the absorbing gas. Of course the SFR per unit H I area would be considerably lower if the star forming region were embedded in a larger H I envelope. Interestingly, at least 50 % of the remaining damped Ly α systems with detected C II* absorption are predicted to have J_{ν}^{stars} within a factor of 3 of the J_{ν}^{stars} inferred for the Q2206A damped Ly α system. It is not clear at this time whether or not their SFRs are within a factor of 3 of the SFR derived for the Q2206A galaxy. We are pursuing a program with the ACS aboard the HST to investigate this question.

The authors wish to recognize and acknowledge the very significant cultural role and reverence that the summit of Mauna Kea has always had within the indigenous Hawaiian community. We are most fortunate to have the opportunity to conduct observations from this mountain. We thank Francesco Haardt and Piero Madau for providing us with their calculations of background intensities and for helpful discussions, and Bruce Draine and Pale Møller for helpful discussions. We thank Dan McCammon for giving us his updated tabulation of X-ray photoionization cross-sections. AMW and JXP are partially supported by NSF grant AST0307824.

REFERENCES

- Bakes, E. L. O. & Tielens, A. G. G. M. 1994, ApJ, 427, 822
 Bennett, C. L., Halpern, M., Hinshaw, G., Jarosik, N., Kogut, A., Limin, M., Meyer, S. S., Page, L., Spergel, D. N., Tucker, G. S., Wollack, E., Wright, E. L., Barnes, C., Greason, M. R., Hill, R. S., Komatsu, E., Nolte, M. R., Odegard, N., Peiris, H. V., Verde, L., & Weiland, J. L., 2003, ApJS, 148, 1
 Blum, R. D. & Pradhan, A. K. 1992, ApJS, 80, 425
 Bruzual, G. & Charlot, S., 2003, MNRAS, 344, 1000
 Churchill, C. W., Vogt, S. S., & Charlton, J. C., 2003, AJ, 125, 98
 Cooke, J., Wolfe, A. M., Howk, J. C., Prochaska, J. X. & Gawiser, E. 2004, in preparation.
 Draine, B. T. 1978, ApJS, 36, 595
 Erb, D. K., Shapley, A. E., Steidel, C. C., Pettini, M., Adelberger, K. L., Hunt, M. P., Moorwood, A. F. M., & Cuby, J.-G. 2003, ApJ, 591, 101
 Field, G. B., Goldsmith, D. W., & Habing, H. J. 1969, ApJ, 155, L149
 Gialisco, M., Dickinson, M., Ferguson, H. C., Ravindranath, S., Kretschmer, C., Moustakas, L. A., Madau, P., Fall, S. M., Gardner, J. P., Livio, M., Papovich, C., Renzini, A., Spinrad, H., & Riess, A. 2004, ApJ, 600, L103
 Haardt, F. & Madau, P. 1996, ApJ, 461, 20
 Haardt, F. & Madau, P. 2003, <http://pitto.mib.infn.it/haardt/cosmology.html>
 Howk, J. C., Wolfe, A. M., & Prochaska, J. X. 2004a ApJ, submitted (astro-ph/0404005)
 Howk, J. C., Wolfe, A. M., Prochaska, J. X. & Gawiser, E. 2004b, in preparation
 Junkkarinen, V. T., cohen, R. D., Beaver, E. A., Burbidge, E. M., Lyons, R. W., & Madejski, G. 2004, ApJ, in press (astro-ph/0407281)
 Kennicutt, R. C. Jr. 1998, ARA&A, 36, 189
 Kulkarni, V. P., Hill, H. M., Schneider, G., Weymann, R. J., Storrie-Lombardi, L. J., Rieke, M. J., Thompson, R. I. 2001, & Jannuzi, B. T. 2000, ApJ, 536, 36
 Kulkarni, V. P., Hill, H. M., Schneider, G., Weymann, R. J., Storrie-Lombardi, L. J., Rieke, M. J., & Thompson, R. I. 2001, ApJ, 551, 37
 Lehner, N., Wakker, B., & Savage, B.D. 2004, preprint
 Machacek, M. E., Bryan, G. L., Meiksin, A., Anninos, P., Thayer, D., Norman, M. L., & Zhang, Y. 2000, ApJ, 532, 118
 Madau, P., Ferguson, H. C., Dickinson, M. E., Gialisco, M., Steidel, C. C., & Fruchter, A. 1996, MNRAS, 283, 1388
 Madau, P., & Pozzetti, L. 2000, MNRAS, 312, L9
 McCammon, D. 2003, private communication
 Miralda-Escudé, J., Cen, R., Ostriker, J. P. O., & Rauch, M. 1996, ApJ, 471, 582
 Mo, H.J., & Miralda-Escudé, J. 1996, ApJ, 469, 589
 Moller, P., Warren, S. J., Fall, S. M., Fynbo, J. U., & Jakobsen, P. 2002, ApJ, 574, 51
 Morrison, R., & McCammon, D. 1983, ApJ, 270, 119
 Motta, V., Mediavilla, E., Munoz, J. A., Falco, E., Kochanek, c. S., Arribas, S., Garcia-Lorenzo, B., Oscoz, A., & Serra-Ricart, M. 2002, ApJ, 574, 719
 Pei, Y. C., Fall, S. M., & Bechtold, J. 1991, ApJ, 378, 6
 Pei, Y. C., & Fall, S. M. 1995, ApJ, 454, 69
 Pettini, M., Smith, L. J., Hunstead, R. W., & King, D. L. 1994, ApJ, 426, 79
 Pettini, M., Shapley A. E., Steidel, C. C., Cuby, J.-G., Dickinson, M., Moorwood, A. F. M., Adelberger, K. L., & Gialisco, M. 2001, ApJ, 554, 981
 Pettini, M., Ellison, S. L., Bergeron, J., & Petitjean, P. 2002, \tilde{a} , 391, 21
 Prochaska, J. X. and Wolfe, A. M. 1997a, ApJ, 474, 140
 Prochaska, J. X. and Wolfe, A. M. 1997b, ApJ, 487, 73
 Prochaska, J. X. 1999, ApJ, 511, 71
 Prochaska, J. X., Howk, J. C., O'Meara, J. M., Tytler, D., Wolfe, A. M., Kirkman, D., Lubin, D., & Suzuki, N. 2002, ApJ, 571, 693
 Prochaska, J. X., Castro, S., & Djorgovski, S. G., 2003 ApJS, 148, 317
 Rauch, M. 1998, ARA&A, 36, 267
 Scott, J., Bechtold, J., Morita, M., Dobrzycki, A., & Kulkarni, V. 2002, ApJ, 571, 665
 Shapley, A. E., Steidel, C. C., Pettini, M., & Adelberger, K. L. 2003, ApJ, 588, 65
 Sheinis, A.I., Miller, J., Bigelow, B., Bolte, M., Epps, H., Kibrick, R., Radovan, M., & Sutin, B. 2002, PASP, 114, 851
 Shull, J. M. & Van Steenberg, M. E. 1985, ApJ, 298, 268
 Steidel, C. C., Adelberger, K. L., Gialisco, M., Dickinson, M., & Pettini, M. 1999, ApJ, 519, 1
 Storrie-Lombardi, L.J., & Wolfe, A. M. ApJ, 543, 552
 Vogt, S. S., Allen, S. L., Bigelow, B. C., Bresee, L., Brown, B., Cantrall, T., Conrad, A., Couture, M., Delaney, C., Epps, H. W., Hilyard, D. F., Horn, E., Jern, N., Kanto, D., Keane, M. J., Kibrick, R. I., Lewis, J. W., Osborne, J. Pardeilhan, G. H., Pfister, T., Ricketts, T., Robinson, L. B., Stover, R. J., Tucker, D., Ward, J., & Wei, M. Z. 1994, SPIE, 2198, 362
 Vladilo, G., Centurion, M., Bonifacio, P. & Howk, J. C. 2001, ApJ, 557, 1007
 Warren, S. 2004, private communication.
 Weingartner, J. C. & Draine, B. T. 2001a, ApJS, 134, 263
 Wolfe, A. M., & Prochaska, J. X. 2000a, ApJ, 545, 591
 Wolfe, A. M., & Prochaska, J. X. 2000b, ApJ, 545, 503
 Wolfe, A. M., Prochaska, J. X., & Gawiser, E. 2003 ApJ, 593, 215 (WPG)
 Wolfe, A. M., Gawiser, E., & Prochaska, J. X., 2003 ApJ, 593, 235 (WGP)
 Wolfire, M. G., Hollenbach, D., McKee, C. F., Tielens, A. G. G. M., & Bakes, E. L. O. 1995, ApJ, 443, 152 (W95)
 Wolfire, M. G., McKee, C. F., Hollenbach, D., & Tielens, A. G. G. M. 2003, ApJ, 587, 278